CHALMERS

Microneurography in conjunction with functional Magnetic Resonance Imaging

Technical Issues and Signal Processing

Master of Science Thesis in Biomedical Engineering

ROKI VIIDIK

Department of Signals and Systems
Division of Biomedical Engineering
CHALMERS UNIVERSITY OF TECHNOLOGY
Göteborg, Sweden, 2010
Report No. EX009 / 2010

Microneurography in conjunction with functional Magnetic Resonance Imaging

Technical Issues and Signal Processing

Roki Viidik

Diploma work No. EX009 / 2010
Department of Signals and Systems
Division of Biomedical Engineering
CHALMERS UNIVERSITY OF TECHNOLOGY
Göteborg, Sweden

Master of Science Thesis in Biomedical Engineering

Performed at: **Sahlgrenska University Hospital**
Göteborg, Sweden
Chalmers University of Technology
SE-41296 Göteborg, Sweden

Supervisor Assoc. Prof. Göran Starck
Department of Medical Physics and Biomedical Engineering
Sahlgrenska University Hospital
Göteborg, Sweden

Examiner: Professor Mikael Persson
Department of Signals and Systems
Division of Biomedical Engineering
Chalmers University of Technology
SE-41296 Göteborg

MICRONEUROGRAPHY IN CONJUNCTION WITH FUNCTIONAL MAGNETIC RESONANCE IMAGING

Diploma work no EX009 / 2010
Department of Signals and Systems
Division of Biomedical Engineering
Chalmers University of Technology
SE-412 96 Göteborg
Sweden
Telephone: +46 (0)31 772 1000

Abstract

Magnetic Resonance Imaging (MRI) is a diagnostic imaging modality that uses a strong static magnetic field in conjunction with gradient fields and RF pulses for obtaining high resolution images from inside of the human body. Functional MRI (fMRI) is a method for imaging brain function with the use of MRI.
Microneurography is an invasive method for recording nerve traffic. It utilizes a thin needle electrode (diameter 200 μm) inserted percutaneously inside a nerve bundle and a reference electrode.
When measuring microneurography simultaneously with MRI, the gradient switching will induce eddy currents in the unavoidable microelectrode loop. The gradient switching signal induced in the microelectrode loop is expected to be several orders of magnitude stronger than the microneurography signal.
The objectives of this study were:

- to investigate the possibility and complexity of recording gradient switching signals in the MR scanner
- assess the maximum signal strength induced in a conducting loop present in the MR bore while scanning
- investigate different possibilities for artefact removal
- investigate the effects of filtering, possible misalignment of the signals etc. on the artefact removal process
- try to remove the gradient switching artefact from an actual microneurography recording
- estimate the requirements for the hardware used in clinical practice.

The measurements were performed at the Sahlgrenska University Hospital MR site (3.0 T Philips Achieva magnet). Matlab was used for calculations and artefact removal algorithms. All measurements were performed one after another with the scanner running the same pulse sequence. The signals were synchronized manually.
The main idea was to record the gradient switching artefact in several positions and/or directions in details and calculate the linear combination of these reference signals by least squares fit to remove the artefact from a signal representing the microneurography recording. No actual microneurography was measured in the MR environment.
The ability to record the gradient switching signals in details was demonstrated with the amplitude being in the same order as the calculated one. The artefact removal was tried by calculating the least squares fit and the effect of different signal processing schemes on the method were investigated. Since the method did not work as good as expected, the possible sources of errors were pointed out and analyzed.
The results are expected to improve significantly when implementing simultaneous measurements. The essence of perfect time alignment was demonstrated. For ideal circumstances where the artefact was synthesized from the reference measurements the method worked nearly perfectly.
As an overall conclusion drawn from the results it must be said that further development of the method is essential. On the other hand, artefact reduction by the factor of 30 was achieved during the tests proving the viability of the idea of calculating linear combination coefficients of reference signals by least squares fit for artefact removal.

Key Words: MRI, fMRI, microneurography, gradient switching, artefact removal.

Acknowledgements

This thesis was written in the Department of Medical Physics and Biomedical Engineering in Sahlgrenska University Hospital under the supervision of Assoc. Prof. Göran Starck. The thesis was written for the Department of Signals and Systems in Chalmers University of Technology. The examiner of this thesis was assigned to be Professor Mikael Persson.

The author of this thesis wishes to express special thanks to Assoc. Prof. Göran Starck for the supervision and support during the measurements, calculations and writing process. Many thanks for the countless revisions of the manuscript and invaluable recommendations.

The author also wishes to express his gratitude to Oskar Talcoth for his guidance, help and comments about the manuscript and for helping to make the thesis correspond to the Chalmers rules.

The author wishes to thank Simon Bergstrand for helping conducting the measurements and Tomas Karlsson for the fruitful ideas and discussions at the meetings. Many thanks go also to Dr. Mikael Elam for initiating the topic and creating the need to investigate this subject.

The author thanks Professor Mikael Persson for offering the thesis and being the examiner.

Special thanks go to Marie Podloucky for being the opponent and withstanding the delays caused by the author.

The author would also like to thank all the MSc and PhD students at Sahlgrenska University Hospital in the Institute of Neuroscience and Physiology for being friendly and supportive, all the teachers and fellow students in Chalmers University of Technology Biomedical Engineering Master Program (year 2008/2009) for being friendly and helpful and making the study period interesting and challenging.

Special thanks go to all Estonians living and studying in Göteborg for making the study period in Chalmers University of Technology so colourful and interesting also outside the school hours.

The author would also like to thank the teachers at Tallinn University of Technology for their support, especially Professor Ivo Fridolin and Viia Roosaar for the support and help when applying for different scholarships that made the study period in Chalmers possible.

Very special thanks to the authors family for the support and guidance that made it possible to come this far and especially for the support and love during the study period at Chalmers University of Technology.

Last, but not the least, the author would like to thank his girlfriend Eha Kulper for being there for him and providing support and consolation.

Table of Contents

1. Introduction

In medicine and medical research, a human is still one of the most investigated subjects. There are many ethical and safety restrictions in investigation of humans. Many of these include the fact that no harm can be made during the studies and all possible safety precautions must be taken. Approval from the local ethics committee is needed for all studies. It is thus very demanding and complicated to do experiments on humans. The safest and least invasive modalities are usually preferred.

The human brain is still a mysterious part of the human being. There is a lot to do before really understanding how it works and in what way different parts of a brain communicate and react. Many applications and post-processing techniques have been developed for performing statistically valid measurements.

One of the safest modalities in modern diagnostic imaging is MRI (which, unlike many others, does not use ionizing radiation for imaging). It uses a strong static magnetic field, referred to as B_0 field, in conjunction with magnetic field gradients (gradient fields) and radiofrequency fields (RF fields) for imaging. This poses some extra requirements on all equipment and electronics used near the scanner in the MR environment.

Magnetic Resonance Imaging has a specialized imaging method called functional MRI (fMRI or BOLD MRI). It gives a possibility to measure the change of activity in different brain regions non-invasively. It has quite good spatial resolution with the voxel size being usually as small as 3^3 mm^3. It has an enormous advantage compared to surface measurements by EEG (electroencephalography) being able to measure activity inside the brain as well. fMRI is used very often in research to determine the activity regions of a brain when performing different tasks.

Microneurography is a method for recording impulse traffic in peripheral nerves of human subjects. It is an invasive method that involves the exploration of very delicate neural structures, nerve fibres, thus having a risk of causing mechanical trauma, intraneural bleedings and infections. [1]

Performing microneurography in conjunction with MRI poses risks that have to be minimized. The electrodes will form a loop that will pick up signals from gradient switching. Since the microneurography signal peaks at about 40 μV and the gradient switching artefact can have peak values up to several hundred mV (depending on the size and orientation of the loop), signal processing is essential for gaining microneurography information.

The objectives of the thesis were:

- to investigate the possibility and complexity of recording gradient switching signals in the MR scanner,
- assess the maximum signal strength induced in a conducting loop present in the MR bore while scanning,
- investigate different possibilities for artefact removal, i.e. find a method to match gradient switching artefact to the reference signals measured elsewhere in the scanner bore,
- investigate the effects of filtering, possible misalignment of the signals etc. on the artefact removal process,
- try to remove the gradient switching artefact from an actual microneurography recording,
- estimate the requirements for the hardware used in clinical practice.

2. Background information and literature study

Magnetic Resonance Imaging (MRI) is, and will continue to be a noble modality in diagnostic imaging and medicine. It utilizes a strong static magnetic field, magnetic field gradients and radio frequency pulses for obtaining high resolution images from inside the human body. It is based on a phenomenon called Nuclear Magnetic Resonance (NMR), discovered by Felix Bloch and Edward Purcell in 1946 [2]. MRI was first demonstrated by Paul Lauterbur in 1973 on small test tube samples using the back projection technique similar to the one used in Computed Tomography (CT). [3]
The year 1975 can be considered as the birth of Magnetic Resonance Imaging as we know it today. It was then when Richard Ernst proposed using phase and frequency encoding and the Fourier Transform. [3]
In 1977 Peter Mansfield developed the Echo-Planar Imaging (EPI) technique that has many applications nowadays, one of them being fMRI (developed in 1992). [3]

2.1 NMR- Origin of the signal

Certain atomic nuclei, when placed in an external magnetic field, align themselves either along or opposite the external field. Due to its large abundance *in vivo*, especially in water and fat, NMR and MRI use most commonly hydrogen ^{1}H nuclei for imaging, with minor exceptions in research.
The alignment of atomic nuclei in a magnetic field is caused by a property called spin. Spin is a fundamental property of nucleons like electrical charge or mass and the spin state can be both positive and negative. It differs between different nuclei and depends on the number of protons and neutrons in this certain nuclei. Individual unpaired electrons, protons, and neutrons each possess a spin of 1/2. Two particles of the same kind can pair up and eliminate the resulting spin to zero. [4]
A particle with a nonzero spin can be considered as a small magnet having a magnetic moment vector with a north and a south pole (Figure 1). In the absence of external magnetic field these nuclei are randomly oriented. On the other hand, when placed in an external magnetic field, this small magnetic moment can be either at a lower energy state, when pointing along the external field, or at a slightly higher energy state, pointing opposite of the external field. At room temperature, the number of spins pointing along the external field (at the lower energy state) is slightly larger than the number of spins pointing opposite the external field (at the higher energy state). This in turn results in a net nuclear magnetisation inside the material, with a magnetic moment **M** (Figure 2). [4]

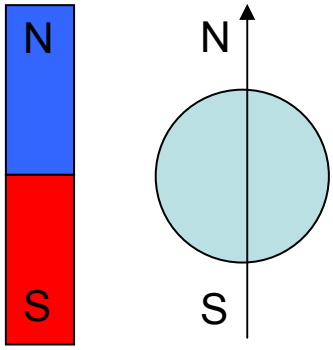

Figure 1: A bar magnet with a north and a south pole, representing a nuclei with nonzero spin.

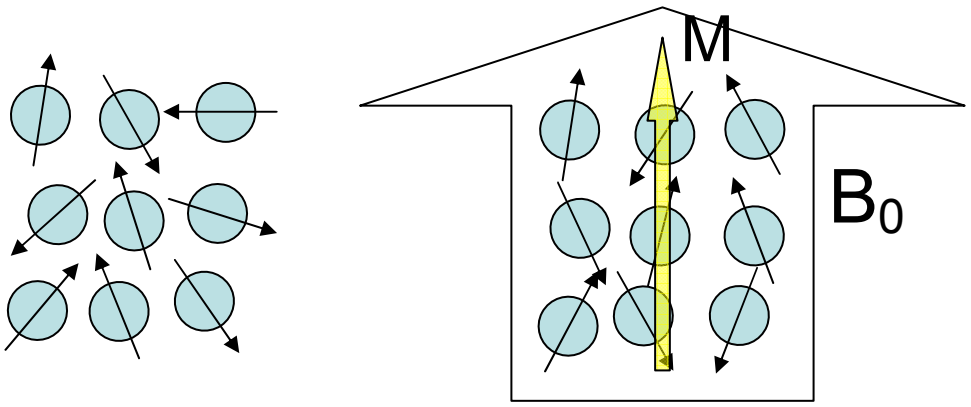

Figure 2: Forming of the magnetic moment vector M.

Originating from the properties of the ^{1}H hydrogen nuclei, the magnetization **M** has an intrinsic precessional motion at the frequency described by the Larmor equation:

$$\omega_0 = \gamma \cdot B_0 \tag{1}$$

where γ is the gyromagnetic ratio and B_0 is the external magnetic field strength.
The strength of the magnetic moment vector **M** depends on magnetic field strength B_0 (that's why stronger field strengths are preferred), square of the gyromagnetic constant γ and the density of ^{1}H hydrogen nuclei P_D,

$$\mathbf{M} = \frac{B_0 \cdot \gamma^2 \cdot \hbar^2}{4 \cdot k \cdot T} \cdot P_D \tag{2}$$

where k is the Boltzmann constant, ħ is the Planck constant and T is the absolute temperature in Kelvin.
It is possible to perform imaging with many isotopes, but due to their large abundance *in vivo* ^{1}H hydrogen nuclei (often denoted as "protons") are usually used for imaging in MRI. The gyromagnetic ratio for protons is γ = 42,58 MHz/T, which means that at the field strength of 3T, the Larmor frequency of protons is ω_0 = 127,74 ≈ 128 MHz.
It is known that when something is precessing or oscillating, it is possible to interact with the system, for example add energy by applying an oscillating force with the same frequency. This phenomenon is known as resonance and it is valid for NMR and MRI as well. Since the oscillation is in the radiofrequency range, a RF pulse can excite the individual protons by taking them to a higher energy state. Macroscopically it turns the net magnetization vector **M** towards the transverse plane. Depending on the strength and length of the RF pulse the resulting net magnetization vector can be on the transverse plane or even point opposite the static magnetic field.
The net magnetization vector **M** has essentially two components. In the resting state, it has only the longitudinal component (parallel to the external magnetic field). When excited, it also has a transverse component orthogonal to the static magnetic field. This orthogonal component is rotating on the transverse plane with Larmor frequency and therefore induces a signal in the nearby coil (Figure 3). This is how the signal is observed both in NMR and MRI.

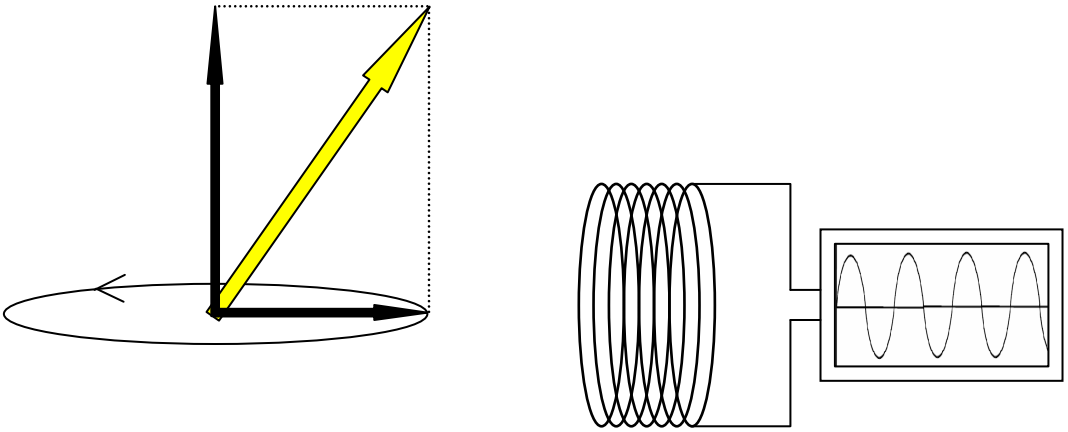

Figure 3: Magnetic moment vector M and its components on the left and the voltage induced in the measuring coil by the transverse component on the right.

After the absorption of energy, when the RF pulse is turned off, the spins will immediately start interacting with each other and with the lattice surrounding them, releasing and radiating some of the energy while returning back to the original, lower energy state. Some of the energy is transformed into heat.
There will be essentially two kinds of relaxation processes taking place. First of them is the spin-spin relaxation, also known as T2 relaxation when different spins interact with each other and exchange energy. The second one is the so-called spin-lattice relaxation or T1 relaxation when the energy is transferred to the surrounding lattices. The two relaxation processes happen simultaneously with different time constants.
T2 relaxation happens with the transverse component of the net magnetization vector **M**. It happens when the spins are oriented in one direction and start to dephase or lose their phase coherence. It can be said that the spins interact with each other or "push" each other out of coherence, thus the name spin-spin relaxation. Figure 4 explains the T2 relaxation with a top view where the $\mathbf{B_0}$ magnetic field is pointing out of the figure.

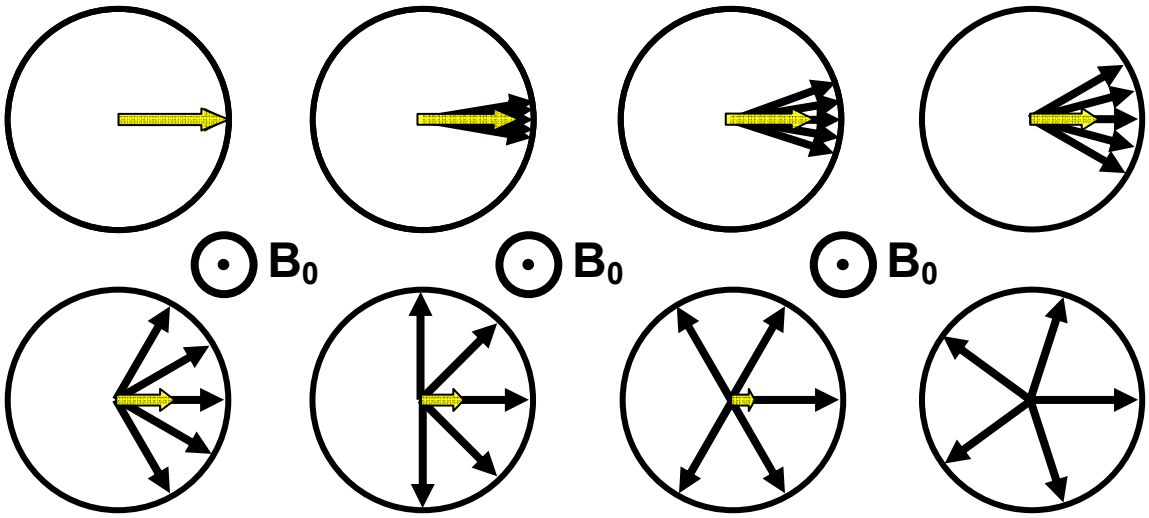

Figure 4: T2 relaxation process where spins lose their phase coherence in the transverse plane. Image represents a top view with the B_0 static field pointing out of the figure.

Due to the inhomogenities in the magnetic field, the loss of phase coherence happens even faster and is called the T2* relaxation. The loss of phase coherence is accelerated.
T1 relaxation, or the spin-lattice relaxation, is the process when the excited spins give energy away to their surrounding tissue (lattice) and return to the lower energy state.

The result of T1 relaxation is the recovery of the longitudinal magnetization. T1 relaxation process is longer than, or equal to, the T2 relaxation for the same substance. Figure 5 presents graphically the proportional loss of transverse magnetization (calculated using T2 time constants) and the recovery of longitudinal magnetization (calculated using T1 time constants) for brain white matter (green), gray matter (orange) and CSF (Cerebra Spinal Fluid, blue). It is assumed that the exciting RF pulse is turned off exactly at time point 0,00.

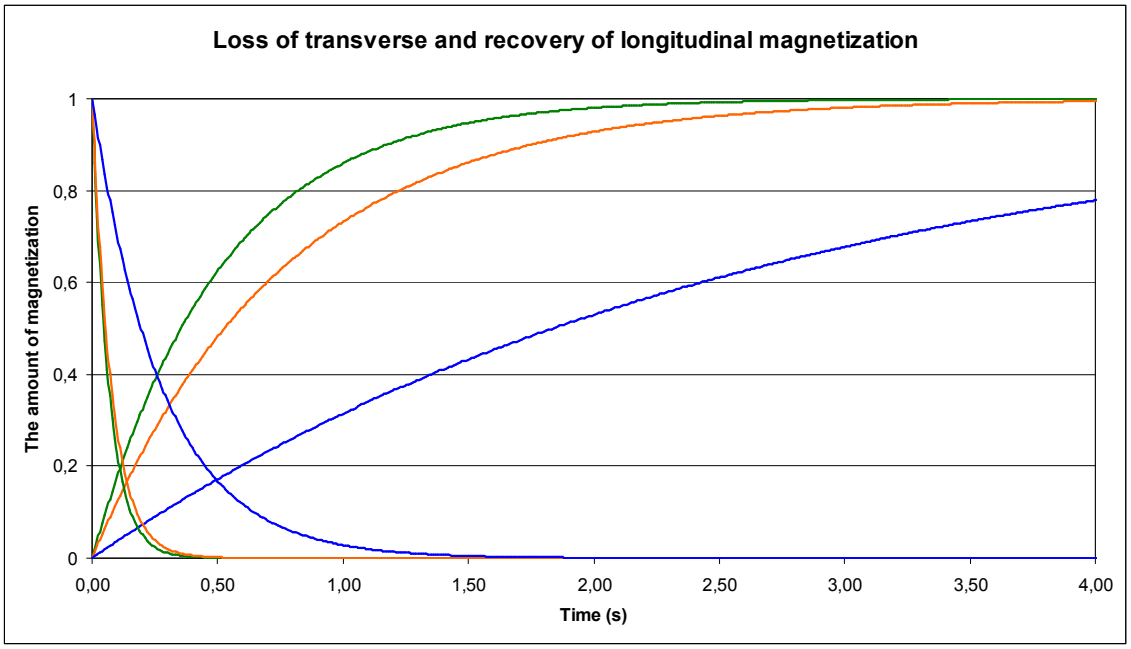

Figure 5: The loss of transverse magnetization (calculated using T2 time constants, Table 1) and the recovery of longitudinal magnetization (calculated using T1 time constants, Table 1) for brain white matter (green), gray matter (orange) and CSF (blue).

During the time constant T2 the transverse magnetization decreases to 37% of its post-excitation value and during T1 longitudinal magnetization recovers to 63% of its initial, before excitation value. Table 1 presents the T1 and T2 values used in Figure 5. [5]

	White matter	Gray matter	CSF
T1	0,51 s	0,76 s	2,65 s
T2	0,067 s	0,077 s	0,28 s

Table 1: T1 and T2 time constants for brain white matter, gray matter and CSF. [5]

The contrast in the image depends on differences in the signal strength. Naturally, different tissue types have different amount of protons, thus resulting in different initial net magnetization. But thanks to different relaxation rates, the signal can be recorded in various ways maximizing the contrast between different tissue types. The time period between the excitation and recording of the signal is called the TE time (Time to Echo or echo time). But different contrast can also be gained by varying the time period to the next excitation, the TR time (Time to Repeat or repetition time). It must be noted that TR is always longer than TE.
If the initial magnetization is the subject of interest (PD or Proton Density imaging), then the signal must be recorded as soon as possible after the excitation to avoid any dephasing (short TE). On the other hand, the time to the next excitation pulse has to be long enough to regain the longitudinal magnetization (long TR).

If one wants to emphasise the difference in the T2 time, the TE must be selected long enough to enable some dephasing, but not too long to risk the loss of magnetization. The TR must be selected also long to regain most of the longitudinal magnetization (long TR, long TE).
For T1 imaging only some of the longitudinal magnetization has to recover. If the longitudinal magnetization has recovered fully in one tissue and only partly in another, before the following excitation pulse is applied, then after the second excitation pulse different tissue types have different amount of transverse magnetisation and the signal must be recorded very quickly (short TE, short TR).

2.2 MRI – How it works

MRI is a medical imaging technique that has the same origin of signal, as NMR. The main difference is that if NMR produces a spectrum from a sample as a result, then MRI is capable of producing images as well. Furthermore, MRI utilizes spatial encoding with gradient fields to determine the location of the measured signal. The switching of the gradient fields, application of the RF pulses and signal sampling is determined by the pulse sequence. Different pulse sequences have different gradient switching schemes along with different TE-s and TR-s resulting in having individual advantages and purposes. Contrast between different tissues can be varied by simply varying the way the image is made.
Due to the fact that hydrogen nuclei, the protons, are the most abundant nuclei in a human body, especially in water and fat, MRI utilizes nearly exclusively protons for imaging, with minor exceptions in the research. A MRI image is actually a map of the local transverse magnetization of the hydrogen nuclei [2].
Most pulse sequences start with a slice selection gradient with a simultaneous RF pulse. Then, the phase and frequency encoding gradients are switched on and off to encode signal inside that slice and the signal is recorded. The procedure is repeated according to the prescribed number of averages for each slice and images are reconstructed.

2.3 Gradient fields

In order to divide the imaging area in smaller regions, gradient fields are used. The smallest volume, corresponding to one pixel in the image, is called a voxel.
Gradient coils are located inside the external magnet. These coils are capable of producing a linear magnetic field gradient in any direction around the isocentre of the magnet. The isocentre is the centre point of the magnet and the magnetic field. It always has the same magnetic field strength since the gradient coils are symmetric about this point and thus produce no change in the magnetic field in the centre of the imaging field. There are three magnetic field gradients for producing orthogonal gradient fields. Each one can have different strength and polarity in different positions inside the scanner bore.
The gradient coils alter magnetic field in space so that it slightly differs in different imaging regions. Since the precession frequency depends on the magnetic field strength, altering the magnetic field will also introduce a small change in the precession frequency. This is the base for spatial encoding in MRI.
In 2D imaging the slice selection gradient is the first one to be applied producing a difference in the Larmor frequency across the imaging field. Then, depending on the desired position and orientation of the slice, a RF pulse with suitable frequency is applied to excite only that one slice. After the RF pulse and slice selection gradient are

turned off, the result is one excited slice having a transverse component of the net magnetization (Figure 6) surrounded by areas that have only the longitudinal component.

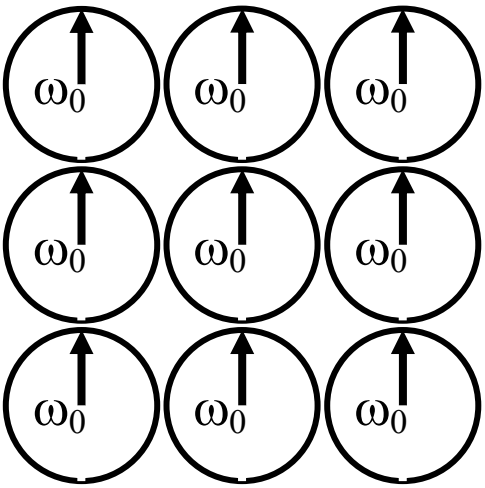

Figure 6: The selected slice after the slice selection gradient and the RF pulse. Note that all the magnetic moments are precessing with the same frequency.

After having an excited slice with all the magnetic moments precessing with the same frequency, a phase encoding gradient is switched on for a short period of time. The phase encoding gradient is orthogonal to the slice selection gradient and it causes a difference in the precession frequency across the slice. This means that different "rows" in the selected slice will have different angles after a certain period of time. Figure 7 shows the effect of phase encoding gradient on the selected slice. The post-excitation magnetization is gray and resulting orientations black. Different precession frequencies ω are also shown.

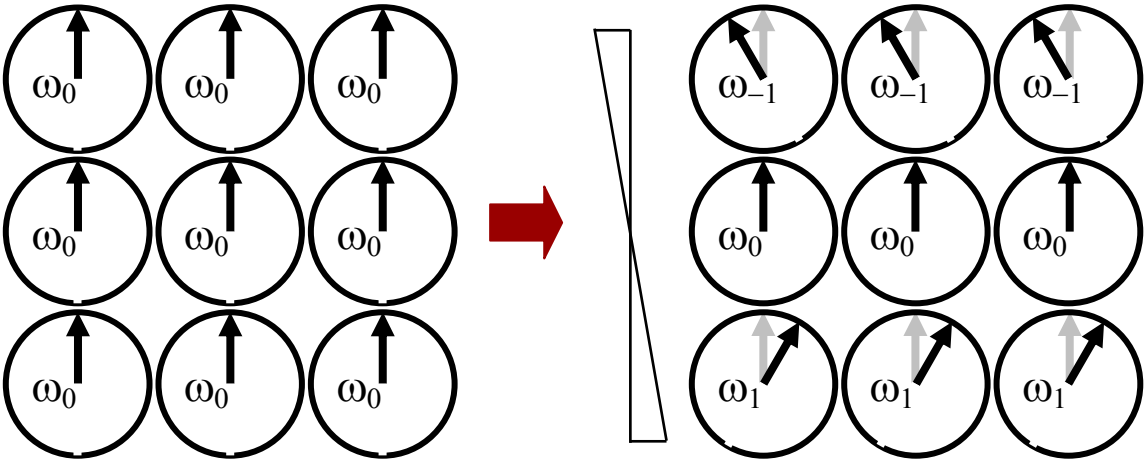

Figure 7: Effect of the phase encoding gradient. The initial transverse magnetization is in gray and the resulting magnetization after the phase encoding gradient, black. Different precession frequencies ω are also visible.

Finally, to be able to distinguish the different voxels along one row, the frequency encoding gradient is applied orthogonally to the slice selection and phase encoding gradients. During the frequency encoding gradient the signal is sampled. Figure 8 shows the effect of frequency encoding gradient resulting in each voxel having its own phase and frequency information. The signal is then sampled in the Fourier domain (having

the phase and frequency information on the axes and amplitude as the value in the matrix) and FFT is used for calculating the final images.

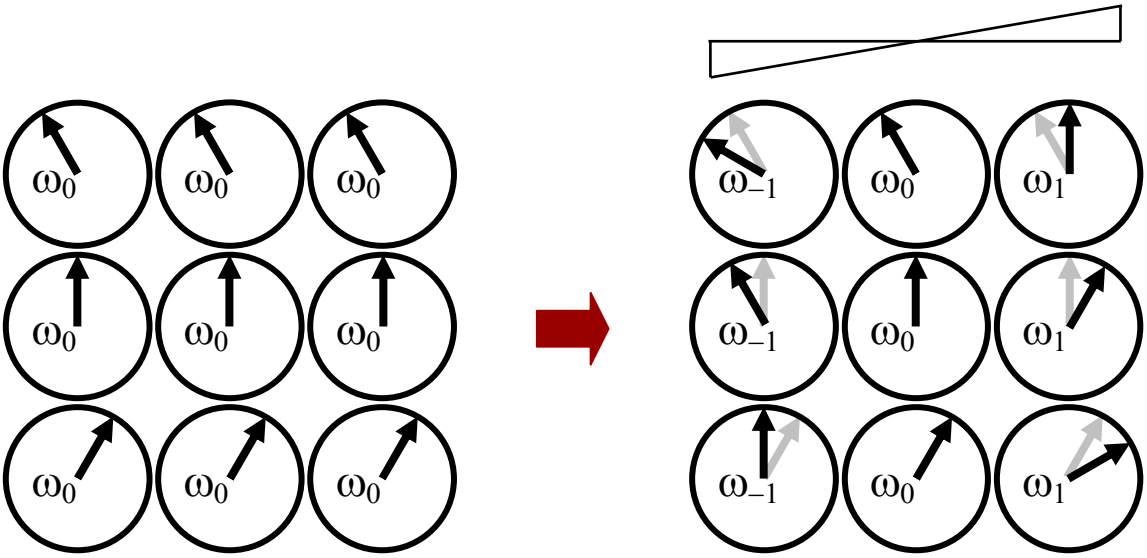

Figure 8: The effect of frequency encoding gradient. Since during frequency encoding gradient the signal is sampled, each voxel will have individual phase and frequency information.

The description above is simplified with a purpose to give the reader an overview about the use of gradient fields. In reality, the use of gradients is more complex and can have more purposes than only the spatial encoding. Usually more than one excitation pulse (among with phase and frequency encoding etc) is required for obtaining one image, making the whole process very time consuming. Fortunately, there are methods for shortening the imaging time remarkably.

2.4 Echo Planar Imaging - EPI

The most commonly used pulse sequence for fMRI is the EPI sequence. It was developed by Peter Mansfield in 1977. It is one of the single-shot techniques which are able to obtain one image in one excitation. Moreover, it is capable of producing many images in just a few seconds.

The EPI sequence used for the experiments is described in Figure 9. It is stimulated by the parameters obtained from the scanner and shows both the RF pulses and the orthogonal gradient fields. The frequency encoding gradient is described as “M”, the phase encoding gradient as “P”, the slice selection gradient as “S” and the RF pulses as “RF_am”.

An EPI sequence usually has a preparation module with a fat suppression pulse [2] (the first, wide RF pulse in Figure 9) followed by the slice selection gradient (the strong slice selection gradient) simultaneously with the excitation pulse (second, short RF pulse). Then, after a short period determined by the TE time, the frequency encoding gradient (during which the signal is sampled) is turned on with rapidly changing opposite polarities. During the changing polarities, phase encoding gradients are turned on for a short period of time as “blips”. It can be imagined that the signal from one slice is sampled row by row, like reading a book (during the frequency encoding gradients) and the phase “blips” are used for changing rows and every second row is read from the end to the beginning. The signal is sampled this way in the Fourier domain and the image is calculated by using FFT.

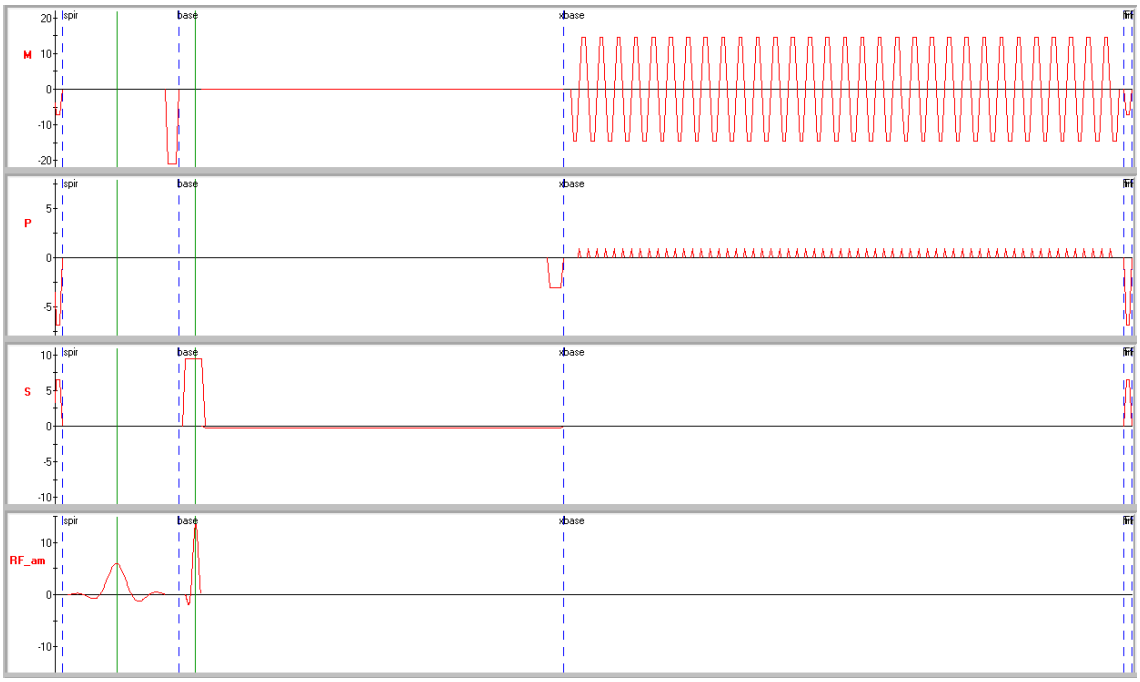

Figure 9: The EPI sequence used for the experiments, stimulated by the parameters obtained from the scanner. It shows both the RF pulses and gradient fields. The frequency encoding gradient is referred to as "M", the phase encoding gradient as "P", the slice selection gradient as "S", RF pulses as "RF_am".

Since the EPI sequence is very fast and utilizes rapid gradient switching, it requires very strong gradient fields that are capable of changing their direction in a very short period of time. The technical limits to the speed of imaging using a single-shot technique is the maximum gradient strength and how fast the gradients can be changed. The gradient amplitudes are measured in milliteslas per meter (mT/m). The stronger the gradient the faster a "row can be read". The measure for the gradient changing direction is measured with two parameters. The slew rate describes the maximum rate of change of the gradient field and is measured tesla per meter per second (T/m/s). The rise time describes the time needed to increase a gradient field from zero to its maximum value, measured in milliseconds (ms). [2]

2.5 fMRI – functional MRI

fMRI or BOLD (Blood Oxygenation Level Dependant) MRI is a method for displaying the activity regions in brain. The activation and rest states are varied in time to gain the signal difference. The difference in signal is caused by variations in regional cerebral blood flow, regional cerebral blood volume and blood oxygenation.
Neuronal activity causes an increase in energy consumption in that specific brain area. This in turn results in two effects also known as hemodynamic response: change in blood oxygenation and increase in blood flow. Hemoglobin is diamagnetic when oxygenated and paramagnetic when deoxygenated. Fully oxygenated blood has about the same magnetic susceptibility as other brain tissues [2]. When the initial concentration of oxygenated / deoxygenated blood is changed, the signal also changes.
The increase in local blood flow usually occurs about one second after the beginning of the activation and peaks in 4-5 seconds. The increase in blood flow is, in fact, larger than the increased energy consumption resulting in the relative concentration of oxyhemoglobin to increase. This in turn results in stronger signal from that brain region. The signal change is in fact so small that it can not be distinguished on regular MRI

images, but since the activation is repeated and correlation between signal strength and activation pattern calculated, the activity regions can be detected.
An fMRI scan is organized in blocks which mean that activation and rest states are alternated and the whole brain is scanned during each block of 3-5 seconds. The voxel size is usually $2^3 – 5^3$ mm^3, resulting in very good spatial resolution.

2.6 Microneurography

Microneurography is a method for recording impulse traffic in peripheral nerves of human subjects. It uses a tungsten microelectrode [1] [7] inserted percutaneously into a nerve. The reference electrode is either a needle electrode inserted under the skin or a surface electrode. [6]
The method utilizing percutaneously inserted tungsten microelectrodes was developed by Hagbarth and Vallbo in 1967 [1]. The use of microelectrodes means that the neural traffic can be recorded both from large myelinated fibres and thin unmyelinated fibres. [6]
The aim of a microneurography study is to measure and record neural traffic in efferent (leading to a muscle fascicle or skin) and afferent (coming from a muscle fascicle or skin) nerves. The neural activity provides, for example, direct information about neural control of autonomic effector organs (including blood vessels and sweat glands). The afferent information is particularly important for the control of precise movements. [6]
The tungsten microelectrode usually has a shaft diameter of 100-200 μm and epoxy varnish as insulation [6]. The electrode impedance can vary strongly being between (0,4) 1 – 5 MΩ at 1 kHz [6]. The insulation from the tip of the microelectrode is peeled off when penetrating the skin.
The signal is recorded as a voltage difference between the intraneural and reference electrode placed usually a few centimetres apart. Band-pass filtering between 500 and 5000 Hz (300 – 5000 Hz [7]) is applied while recording the signal [6]. The traditional analysis of sympathetic bursts includes it being passed through a leaky integrator with a time constant of about 100 ms. The result is a mean-voltage neurogram from where the number of visible bursts is counted. The burst frequency (number of bursts per minute) or burst incidence (bursts per hundred heartbeats) is calculated [7].
As being an invasive method that involves the exploration of very delicate neural structures, nerve fibres, performing microneurography has a risk of causing mechanical trauma, intraneural bleedings and infections [1].
Figure 10 shows an example of a microneurography signal recorded at Sahlgrenska University Hospital with a sampling frequency of 25641 Hz. Figure 11 shows a band-pass filtered, rectified and smoothed result of the same signal. The distinguishable peaks on Figure 11 are the bursting periods. Each peak corresponds to one bursting period.

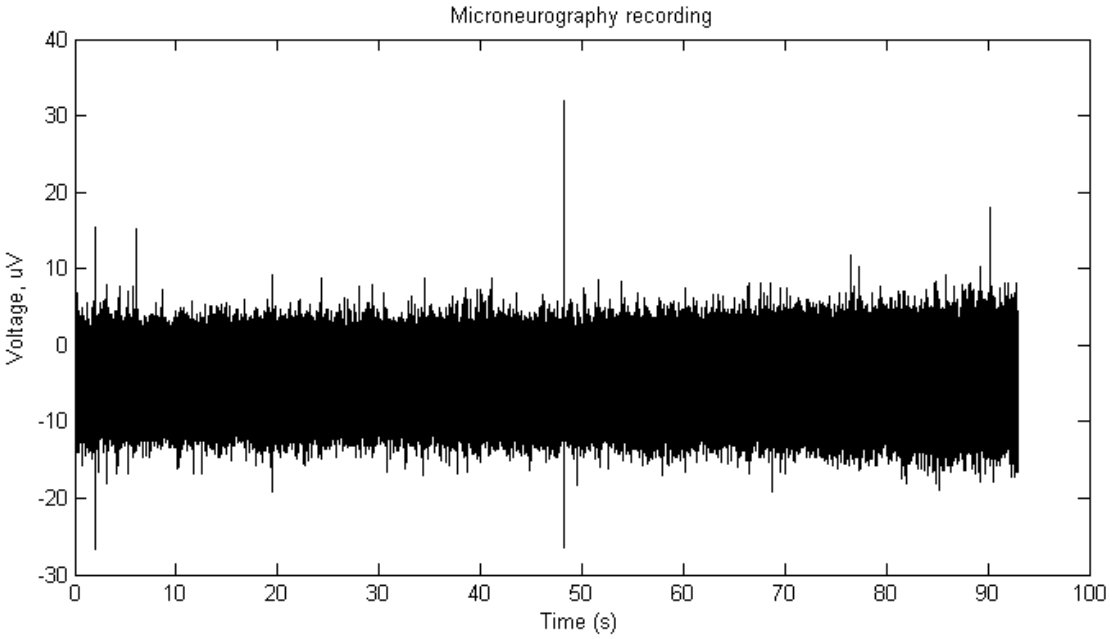

Figure 10: Example of a microneurography recording from Sahlgrenska University Hospital.

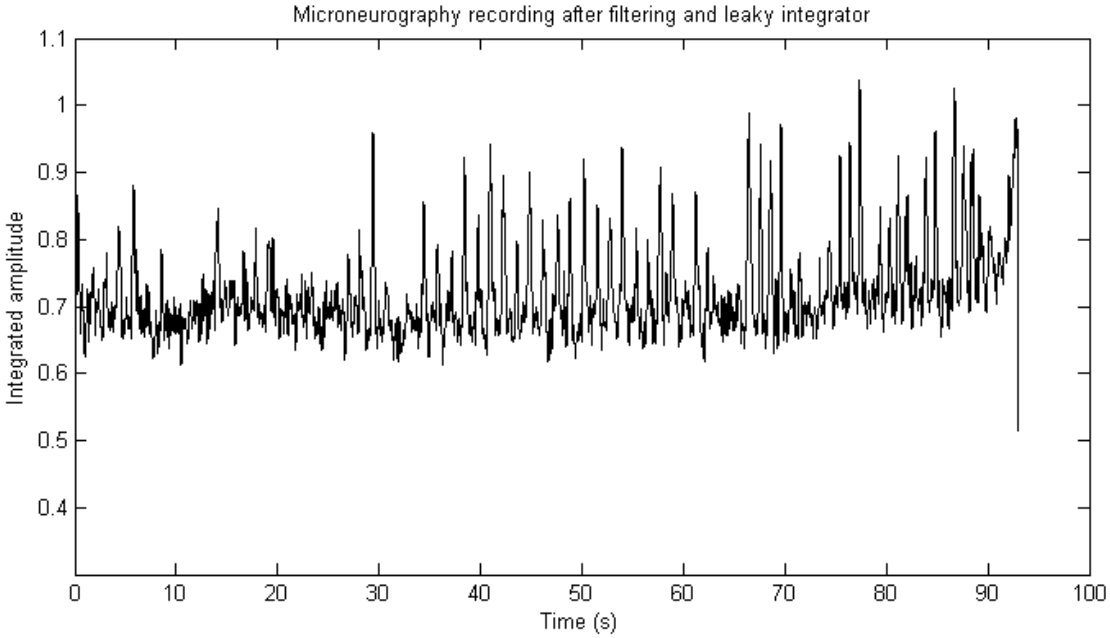

Figure 11: Example of a band-pass filtered, rectified and smoothed microneurography recording from Sahlgrenska University Hospital. The distinguishable peaks are the bursting periods. Each peak corresponds to one bursting period.

3. Methods

All measurements were performed at Sahlgrenska University Hospital on a Philips Achieva 3.0T magnet (Philips Medical Systems, Best, The Netherlands). The set up included a phantom inside the head coil and different custom made coils for collecting the signals. The pulse sequence used for the measurements was an EPI sequence usually used in fMRI studies. FOV = left-to-right: 200 mm; anterior-to-posterior: 240 mm; feet-to-head: 148 mm, TR = 3500 ms, TE = 35ms, Flip Angle = 90°, 53 transversal slices, scan voxel size = 2.8 x 2.8 x 2.8 mm^3. The slices were always set orthogonal with the magnetic field. Gradient mode was set to maximum and peripheral nerve stimulation (PNS) mode was set to "high".
The cables from the coils were placed as close to the symmetry axis of the magnet as possible. All loops were taken as far from the magnet as possible.
All measurements were performed one after another with the scanner running the same pulse sequence. The signals were synchronized manually by correcting the time alignment for the spoiler gradient pulse.

3.1 Signal processing

There are three orthogonal gradient fields in a MR scanner. Each of them is used while scanning and encoding the signal. The gradients have a linear region about the isocentre of the magnet extending about 25 cm on both sides of the magnet's symmetry axis (the z-axis). The longitudinal gradient alters the magnetic field along the isocentre axis and transverse gradients along the corresponding orthogonal axes.
A microneurography recording set-up includes an unavoidable loop area. The size and orientation of this loop can not be predicted since finding the nerve fibres is a delicate and time-consuming process. After finding the nerve and gaining enough signal strength, the electrodes are left as they are and not moved thereafter. When the microneurography recording is performed in the MR environment, this electrode loop will pick up the gradient switching signal as well as the neural traffic signal. The amount of each gradient signal being present in the recording depends on the size and orientation of the loop area and differs from subject to subject.
By knowing the exact waveform of each gradient field, it is possible to find a combination of these three fields that minimizes the gradient switching signal on the microneurography recording.
It is really difficult, if not impossible to have the perfect positioning and orientation of the reference coils for picking up each of the gradient waveforms individually. Each gradient produces a small change in magnetic field in other directions as well (due to the coil configuration that attempts to produce as linear field as possible about the isocentre). The exact gradient coil winding structures and the way pulse sequences are played out is usually classified information by the MR scanner vendors making it difficult to perform accurate simulations of the gradient fields.
Alternatively, measurements of reference signals at three properly selected positions distant from each other (maximizing the signal differences, Figure 12) can be used instead of three individual gradient waveforms. These reference signals each include a unique combination of the gradient fields which together contains all the information about gradient field waveforms in different directions.
One of the main points of the thesis is to record the three reference signals at the rear side of the magnet. That is because the microneurography examination includes measuring additional physiological properties as well, e.g. blood pressure, ECG,

breathing, sweating (impedance of the skin) etc. There will be many devices present around the patient which means that by performing the reference signal measurements on the rear side, we minimize the possibility for artefacts that arise from movements of the coils.

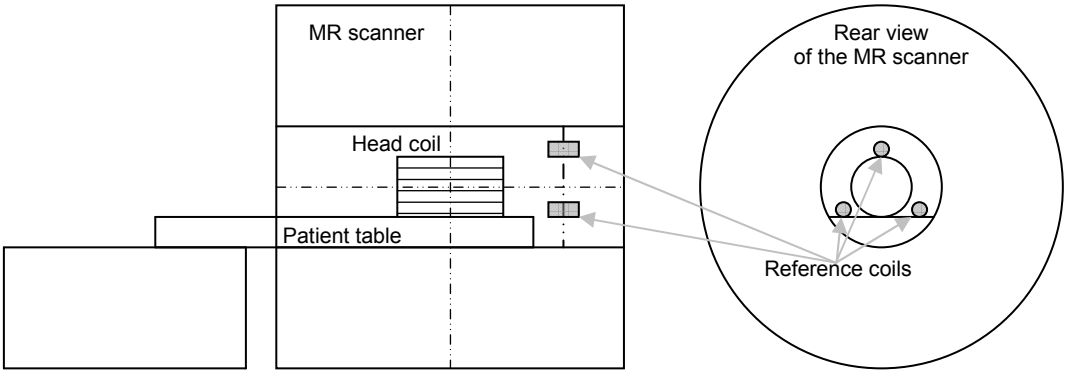

Figure 12: A schematic description of the three reference coils and their position in the MR scanner.

A fourth reference signal can be measured as a supplementary signal at the electrode loop by having a single wire following the wires to the electrodes. It will not have exactly the same loop area and orientation, but it can be used as additional information about the gradient switching signal picked up by the electrodes when the artefact removal process is insufficient.

The aim of this thesis was to investigate the method and problems of calculating linear combination coefficients by least squares fit for a signal imitating the gradient switching picked up by the microneurography electrode loop, which can also be called an artefact signal **a**, with the use of Matlab. The corresponding combination of reference signals should be identical to **a** resulting in a zero signal after subtraction. Unfortunately, noise and slight misalignment of the signals in time might result in a remaining signal that will corrupt the microneurography information.

The gradient switching signal picked up by the coil imitating the electrode loop can be considered as an artefact vector **a**. It consists of a linear combination of three reference signals, $\mathbf{r_1}$, $\mathbf{r_2}$, $\mathbf{r_3}$ and the error term **e**.

$$\mathbf{a} = c_1\mathbf{r}_1 + c_2\mathbf{r}_2 + c_3\mathbf{r}_3 + \mathbf{e} \tag{3}$$

where c_1, c_2 and c_3 are the linear combination coefficients and **e** is the comprehensive effect of noise.

Formula (3) can be rewritten as:

$$\begin{bmatrix} a_1 \\ a_2 \\ a_3 \\ \vdots \\ a_l \end{bmatrix} = \begin{bmatrix} r_{11} & r_{21} & r_{31} \\ r_{12} & r_{22} & r_{32} \\ r_{13} & r_{23} & r_{33} \\ \vdots & \vdots & \vdots \\ r_{1l} & r_{2l} & r_{3l} \end{bmatrix} \begin{bmatrix} c_1 \\ c_2 \\ c_3 \end{bmatrix} + \begin{bmatrix} e_1 \\ e_2 \\ e_3 \\ \vdots \\ e_l \end{bmatrix} \tag{4}$$

which in turn can be written in a more compact way as

$$\mathbf{a} = \mathbf{R}\mathbf{c} + \mathbf{e} \tag{5}$$

where **R** is a matrix with reference signal $\mathbf{r}_1$ in the first, $\mathbf{r}_2$ in the second and $\mathbf{r}_3$ in the third column, **c** is a column vector consisting of the linear combination coefficients for the reference signals.

In order to get the coefficients **c**, the following equation must be solved:

$$\mathbf{R}^T\mathbf{a} = \left(\mathbf{R}^T\mathbf{R}\right)\mathbf{c} \tag{6}$$

Given that $\mathbf{R}^T\mathbf{R}$ is invertible, **c** can be estimated as:

$$\mathbf{c} = \left(\mathbf{R}^T\mathbf{R}\right)^{-1}\mathbf{R}^T\mathbf{a} \quad (7)$$

The method described above is known as the General Linear Model (GLM) [9]. It is an extension to the Multiple Regression theory where the best prediction of the dependent variable, in our case artefact signal **a**, is given with a combination of the independent variables, reference signals $\mathbf{r}_1$, $\mathbf{r}_2$, $\mathbf{r}_3$. The deviation between the artefact signal points and its predicted values is called the residual signal. The goal of linear regression is to find the least squares estimation for the residual signal which means that the predicted signal is fitted as close as possible to the artefact signal. [9]

One of the advantages the GLM has over Multiple Regression is that it is able to provide a solution even when the $\mathbf{r}_1$, $\mathbf{r}_2$, $\mathbf{r}_3$ variables are not linearly independent [9].

For calculating the coefficients **c** (formula 7), a Matlab command backslash ("\") or matrix left division is used. It calculates the solution in the least squares sense to the under- or overdetermined system of equations [8]. Since the calculation finds the least squares solution, it can be applied for the trials with artefact signal including microneurography as well.

In order to have as little effect from the microneurography signal on the linear combination method as possible, the system has to be well overdetermined. The motivation is that the bursting activity is the signal of interest in the microneurography recording, and these bursts occur independently of the gradient switching, the level of overdetermination must rule out all the possibilities of the gradient switching being accidentally synchronized with the bursting activity. Additionally, going to the limit of using only three samples for the reconstruction, the residual signal would be suppressed to zero.

The electromotive force (*emf*) induced by the gradient switching in the coils can be calculated with the formula

$$emf = \frac{d\Phi}{dt} = \frac{d\left(B \cdot A\right)}{dt} = A \cdot \frac{dB}{dT} \quad (8)$$

where Φ stands for the magnetic flux, B is the magnetic field and A is the loop area of the coil.

Table 2 presents the information about the MR system [11].

Mode	Parallel / Sequential
Maximum Gradient Amplitude	40 / 80 mT/m
Maximum Slew Rate	200 / 100 T/m/s
Minimum Rise Time	0.2 / 0.8 ms

Table 2: Details of Philips Achieva 3.0T magnet (Philips Medical Systems, Best, The Netherlands). [11]

It must be noted that the strength of the dB/dt signal depends on the steepness of the gradient and varies for different pulse sequences. Since the EPI pulse sequence is a single-shot imaging method, it is expected to have gradient slew rate close to the maximum values.

3.2 Measurements on RF and Gradient fields

An Agilent 54621A oscilloscope was used for viewing the waveforms (input resistance 1MΩ±1%, capacitance 14 ~pF) [10]. A custom made coil (Figure 13) with 100 windings was used for picking up the signals. The diameter of the coil was measured to be 46 mm making the effective area of one turn 16,62 cm^2. This makes the effective area of the whole coil about 0,166 m^2. The normal of the coil loops was always set parallel to the main magnetic field.
Measurements were performed at two positions. First ones at about 25 cm from the isocentre and second ones at the approximate position of a medium-height patient knee (close to the entrance of the MR bore). All measurements were made as close to the magnet symmetry axis as possible.

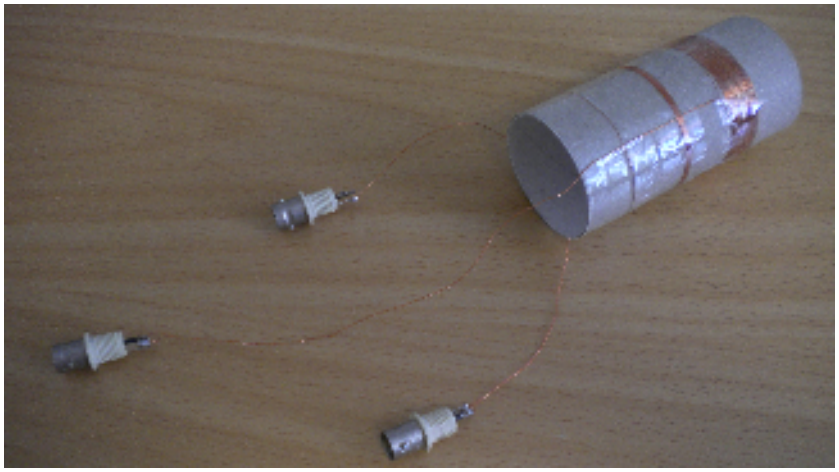

Figure 13: The coil used for the measurements. (Left one has one turn, middle one 10 and right one has 100 turns.)

The aim of the first measurement session was to determine the suitability of the custom made coils for signal registration during the following experiments in the MR environment. The possible precision of the recordings and the signal strength had to be noted. Photographs of the interesting parts of the EPI sequence were taken from the oscilloscope screen. An overview about the equipment requirements needed for future measurements was obtained.
Knowing the maximum slew rate of 200 T/(m·s) (from Table 2) and the distance from the isocentre of ¼ meters, the theoretical maximum induced voltage in the coil was expected not to exceed (formula 9):

$$emf = A \cdot \frac{1}{4} \cdot \frac{dB}{dT} = 0{,}166 \cdot \frac{200}{4} = 8{,}3V \ .$$

3.3 Artefact amplitude measurements

Measurements were performed using a DT9802 ADC by Data Translation (Marlboro, Massachusetts, USA) with 50 kHz sampling frequency and 12-bit signal depth (input impedance 100 MΩ, 100 pF) [12]. The custom made coil with 100 turns was used for collecting the signals.
The measurements were performed on the z-axis of the magnet at positions 25, 50, 75, 95, 110, 125, and 140 cm from the isocentre. The normal of the coil loops was parallel to the main magnetic field. All measurements were performed on the magnet symmetry axis.

The signal from the 10 first volumes of the EPI sequence was recorded (about 30 seconds), and the seventh volume was analyzed. Then, the amplitude of the gradient peaks was assessed. The frequency content of the signal was also observed with the use of FFT.
The main purpose of this measurement set was to obtain information about the gradient field distribution inside and close to the magnet. We also wanted to compare our measurement results with [11] (An Investigation into Occupational Exposure to Electromagnetic Fields for Personnel Working With and Around Medical MRI Equipment).

3.4 Measurements at the rear side of the magnet. Testing linear combination for artefact removal

Measurements were performed using a DT9802 ADC by Data Translation (Marlboro, Massachusetts, USA) with 50 kHz sampling frequency and 12-bit signal depth (input impedance 100 MΩ, 100 pF [12]). The custom made coils with 100 and 10 turns were used for collecting the signals. Additionally, a 100 turn coil with additional 430 kΩ resistor added in series was tested.
All together 4 signals were measured at the rear side of the magnet with a 100 turn coil and 4 signals were measured in front of the magnet with a 10 turn coil. The signals measured at the rear side are used as reference signals for calculating the linear combinations to reproduce the signals measured on the front side (imitating the artefact signals). The residual signal after artefact removal (obtained by subtracting the reproduced signal from the original artefact signal) includes the noise and inaccuracy of the linear combination method. The residual signal is evaluated with its maximum absolute and RMS value. These values are compared with the corresponding resulting signal values. Before any other calculations, the DC offset was removed from all of the references and signals by subtracting the mean value.
The coil positions are described in Figure 14. The coils on the rear side of the magnet were placed in a triangular shape to maximize the difference of the recorded signals. One of the reference recordings were performed with the coil placed as far inside the scanner bore as possible. This is the place where the signal with 100 turn coil and 430 kΩ resistor was also measured. The signals from the front of the magnet were measured at the entrance of the bore to imitate the possible position of the microneurography electrode loop. The distance from the isocentre is similar to an average patients' knee position when performing the brain examination.
Reference 1 was recorded approximately 13 cm above the magnet symmetry axis (z-axis), reference 2 approximately 17 cm below and 20 cm left from the symmetry axis and reference 3 approximately 17 cm below and 20 cm right from the symmetry axis. Reference 1, 2 and 3 were all obtained about 10 cm in from the magnet end plane. Reference 4 and the measurement with the 430 kΩ resistor were measured 17 cm below and 20 cm right from the symmetry axis and 25 cm in from the magnet end plane. Reference 2, 3 and 4 were in direct contact with the magnet cover during the measurements.
Signals 1, 2, 3 and 4 were all measured with the 10 turn coil approximately 20 cm above the MR table. The first one was 5 cm in and others 10 cm out from the magnet end plane. Signals 1 and 2 were 15 cm from the magnet symmetry axis at the approximate position of a patients left leg. Signals 3 and 4 were on the symmetry axis. For measuring signal 4, the coil was tilted 45° on the horizontal plane.

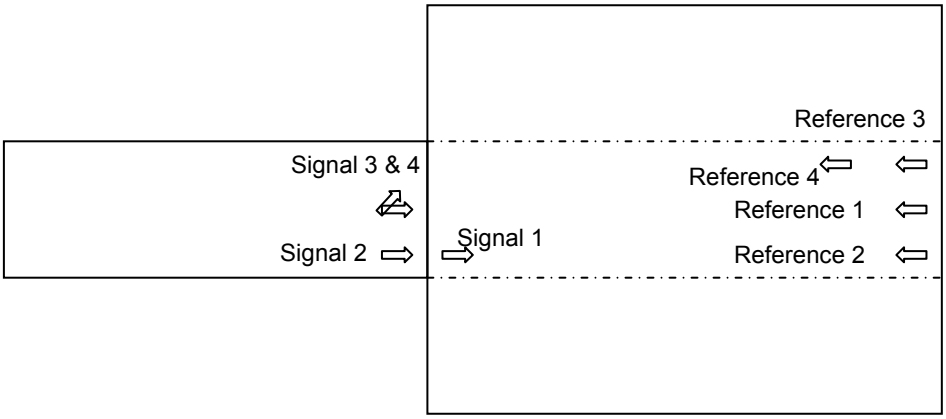

Figure 14: Coil positions for the third measurement set. Reference 1 was recorded approximately 13cm above the magnet symmetry axis (z-axis), reference 2 approximately 17 cm below and 20 cm to the left from the symmetry axis and reference 3 was approximately 17 cm below and 20 cm right from the symmetry axis. Reference 1, 2 and 3 were all obtained about 10 cm from the magnet end plane. Reference 4 was measured 17 cm below and 20 cm to the right from the isocentre axis and 25 cm in from the magnet end plane. Reference 2, 3 and 4 were in direct contact with the magnet cover during the measurements.
Signals 1, 2, 3 and 4 were all measured with the 10 turn coil approximately 20 cm above the MR table. The first one was 5 cm in and others 10 cm out from the magnet end plane. Signals 1 and 2 were 15 cm from the magnet symmetry axis at the approximate position of a patients left leg. Signals 3 and 4 were on the symmetry axis. For measuring signal 4, the coil was tilted 45° on the horizontal plane.

All measurements were performed one after another with the scanner running the same pulse sequence. The same 100 turn coil was used for recording all reference measurements and the same 10 turn coil for all artefact measurements.
The signal from 10 first volumes of the EPI sequence was recorded (about 30 seconds), and the seventh volume analyzed. The synchronisation was achieved manually by plotting and shifting the results. A set of reference measurements was chosen (3 or 4) and linear combination calculated for each of the signals 1-4. Then, the resulting signals were calculated using the linear combination coefficients and corresponding reference signals. After subtracting the calculated signal from the original signal, maximum absolute and RMS values of both the signal and final result were calculated using Matlab commands “max”, “abs”, “dot”, “sqrt” and “length”. Amplitude and RMS reduction was obtained by dividing the corresponding maximum values.

$$\max value = \max(abs(signal)); \tag{9}$$

$$RMSvalue = \max(sqrt(dot(signal, signal)/length(signal))); \tag{10}$$

The possible error caused by misalignment of signals in time was investigated. For that, a time-shifted copy of the signal was generated with the Matlab command “interp1”. It uses linear interpolation for creating additional data points between the initial ones at specified positions.

$$Shiftedsignal = interp1(signal,datapoints,shiftedpoints,'linear'); \tag{11}$$

The shifted signal was subtracted from the original and maximum absolute values calculated (formula 11). By dividing the values, relative amplitude difference was obtained.
In order to verify the linear combination method and see how well it works in an ideal situation where a perfect combination exists, a synthesized signal was made composing of a linear combination of three reference signals (Reference 1, 2 and 4) multiplied with coefficients [3.1337, 0.1337, 5.3533]. The post-processing and result evaluation was performed the same way as for the previous calculations.

To make the ideal situation more complicated and see the possible effect that the signals from the same frequency range as the gradient switching have on the linear combination method and *vica versa*, a test was made where periodic sine and cosine signals were added to the same synthesized signal. Matlab commands "sin_tr" and "cos_tr" were used for producing the oscillations. The magnitude of the artificial sine and cosine signals was chosen about 100 times less than the synthesized signal amplitude. Two tests were done with the first one having approximately 76% of amplitude of 950 Hz cosine and 24% of 2200 Hz sine signal. The second had approximately 63% of amplitude of 975 Hz cosine and 37% of 1200 Hz sine signal. The post-processing and result evaluation was performed as for the previous calculations. The same was done with a real microneurography signal as the third test.
Since the measurements were performed semi-simultaneously and a slight misalignment of maximum half a sample, or 10 µs, might still be present between the recordings, the effect of smoothing prior to linear combination calculations was tried. Both the effect of low-pass and high-pass filters was investigated. Matlab command "buttord" was used for calculating the order of the filter and natural, or 3dB, frequency, "butter" for designing the Butterworth filter and "filter" for filtering. The linear combination calculations and post-processing with result evaluation was performed the same way as for the previous calculations.
For low-pass filtering the pass-band corner frequencies of 6500, 10000 and 13000 Hz were used. The stop-band corner frequencies were 10000, 13000 and 20000 Hz, respectively. For high-pass filtering, the pass-band corner frequencies of 700, 500 and 300 Hz were used and a stop-band corner frequency of 50 Hz was used for all cases. The pass-band ripple of 3 dB was allowed and stop-band attenuation of 20 dB required for all filters.

3.5 Measurements with the stands and new coils

To avoid mechanical vibrations from the MR scanner covers in the measuring coil, new measurements with two stands (Figure 15) and a coil support attached to the stands (Figure 16) were performed. The stands were positioned on the floor and additional weight was applied to make the set-up more stable. The measuring coils had no direct mechanical connection to the magnet cover. The stands and the coil support were fully made of wood.
Signals were recorded with a DT9802 ADC by Data Translation (Marlboro, Massachusetts, USA) with 100 kHz sampling frequency and 12-bit signal depth (input impedance 100 MΩ, 100 pF). The motivation for using higher sampling frequency was to record the waveforms more precisely increasing the precision of the linear combination result.
Orthogonal coils (Figure 16) were used for the measurements. This offered an opportunity to measure all three orthogonal components of the gradient fields.
The diameter of the coils was measured to be 33,8 mm. This makes the area of one turn 897.3 mm^2 and the whole coil 8.9727 dm^2 or 0.0897 m^2.
The orthogonal gradient switching signals were measured at several positions, but only the ones measured closest to the head coil on the magnet symmetry axis and the ones measured in front of the magnet at approximate knee position were used for the calculations.
Three sets of orthogonal signals (not used in the thesis) were measured at approximately 35 cm from the isocentre plane where, according to [11], the amplitude of the gradient switching has its maximum. Fourth set of reference signals was measured as close to the head coil as possible, with the closest coil being only 2 cm away from the tip of the

head coil, about 20 cm from the isocentre of the magnet. Two sets of signals were measured at the front side of the magnet. One approximately on the symmetry axis about 20 cm out of the magnet end plane (not used in the thesis) and the second at the approximate position of a tall patients left knee, about 10 cm out of the magnet end plane and 15 cm right from the symmetry axis (when facing the magnet).
All measurements were performed one after another with the scanner running the same pulse sequence. Between measuring the orthogonal components of the gradient switching at a specific position, the ADC was disconnected from the previous coil and connected to a new coil. The coil supports were not moved in between the measurements of the same position.
The signal from 10 first volumes of the EPI sequence was recorded and the seventh volume analyzed. The synchronisation was achieved manually.

Figure 15: The stands, the coil support with the coils and a stabilizing weight mounted in front of the scanner.

The set of orthogonal signals measured at the rear side of the magnet close to the head coil and symmetry axis of the magnet were chosen as reference measurements. The orthogonal signals measured at the approximate knee position were chosen as artefact signals. The linear combination coefficients were calculated for each of the artefact signals separately. The resulting signal was subtracted and the results assessed with the maximum absolute values and RMS values of the signals and results and their respective reduction factors. The calculations were performed according to formulas (9) and (10).
To see the possible residual time misalignment and improvement of adding slightly time shifted copies of the reference signals to the calculations, two additional reference signals were calculated for each orthogonal reference signal with formula (11). One was

shifted by 0,1 sample before and the other by the same shifting factor later. The results were assessed as before.
A test was made with the artefact signal that seemed mostly out of synchronization where it was shifted by one sample to the other side of "ideal" synchronization. The linear combination and other calculations with the results assessment was done as before. Both the set of three and the set of nine reference signals were used for reconstructions and the results compared.

Figure16: The orthogonal coils at one end of the coil support.

The microelectrode loop area will be about 2 dm^2 in a microneurography measurement situation. To get a fairly bad estimation of the artefact signal, the orthogonal components measured at the knee position were divided by 5 to correspond to the approximate loop area of 1,8 dm^2 in each direction and added together as the artefact signal. An upsampled version of microneurography (using formula 13) with some bursting activity was added to the calculated artefact signal and reconstructions tried with nine reference signals. Different amplification of the microneurography signal prior to adding the artefact signal was tried and SNR estimated for each case (formula 14). The artefact signal without the added microneurography was taken as the supplementary signal from the electrode loop following the microelectrode loop.
The SNR (Signal to Noise Ratio) of two signals is defined as the power of the signal divided by the power of noise. If the lengths of the signals are the same, it can be calculated as the square of the RMS difference (RMS of the signal divided by the RMS of noise):

$$SNR = \frac{P_{signal}}{P_{noise}} = \left(\frac{RMS(amplitude)_{signal}}{RMS(amplitude)_{noise}} \right)^2 \qquad (12)$$

The linear combination coefficients along with the corresponding signals were calculated for microneurography with added artefact and supplementary signal. After artefact subtraction, the results were filtered with a Butterwoth filter similar to the one used in clinical practice and the moving average was calculated. For some amplification levels, the supplementary signal final result was subtracted from the microneurography final result.
Additional tests with the microneurography signal magnified by 10, 100, 1000 and 10000 times of its initial value were performed.

4. Results

The following chapter presents results from the measurements and calculations described in chapter 3 in the form of images, graphs, tables and descriptive text.

4.1 Measurements on RF and Gradient fields

During the first measurement set the oscilloscope with 200 MHz sampling frequency was used for visualizing the signals. Since the Larmor frequency of protons at 3T is about 128 MHz, the aliased version of RF pulses could be seen (the envelope of the signals is clearly visible).
Figure 17 shows the induced voltage in the coil during one slice of the EPI sequence. The coil was positioned on the symmetry axis of the magnet about 25 cm from the magnetic field isocentre. It can be seen that the RF pulse and gradient switching both induce the maximum peak to peak voltage of about 3,5 V.

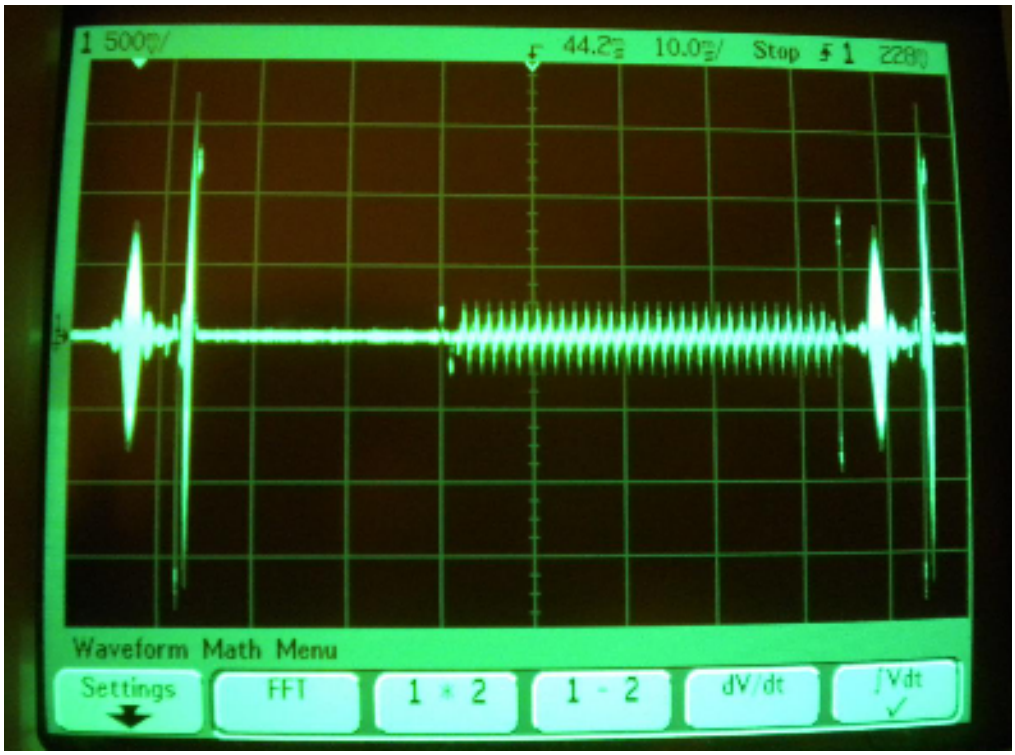

Figure 17: dB/dt of the EPI pulse sequence for acquiring one slice. The coil was on the symmetry axis of the magnet about 25 cm from the isocentre. On the left the lipid suppression pulse can be seen followed by a slice selection gradient and RF pulse which are closely together. After about 30 ms, the readout part of the pulse sequence can be recognized (a sum of phase and frequency encoding gradients). The horizontal scale is 10 ms per square and vertical 500 mV per square.

Figure 17 can be compared to Figure 9 and different parts of the signal can be recognized. The first, wide RF pulse is the spectrally selective pulse for suppressing the lipid signals (can also be seen in Figure 18 in more detail). Next, the slice selection gradient is turned on and slice selective RF pulse can be seen. Then, the slice selection gradient is turned off and after a short "silent" period, the rapid gradient switching begins. This is the readout part of the sequence composing of phase and frequency encoding gradients. During this time the MR system records the image. In the end a spoiling gradient can be seen and then the next slice is acquired.

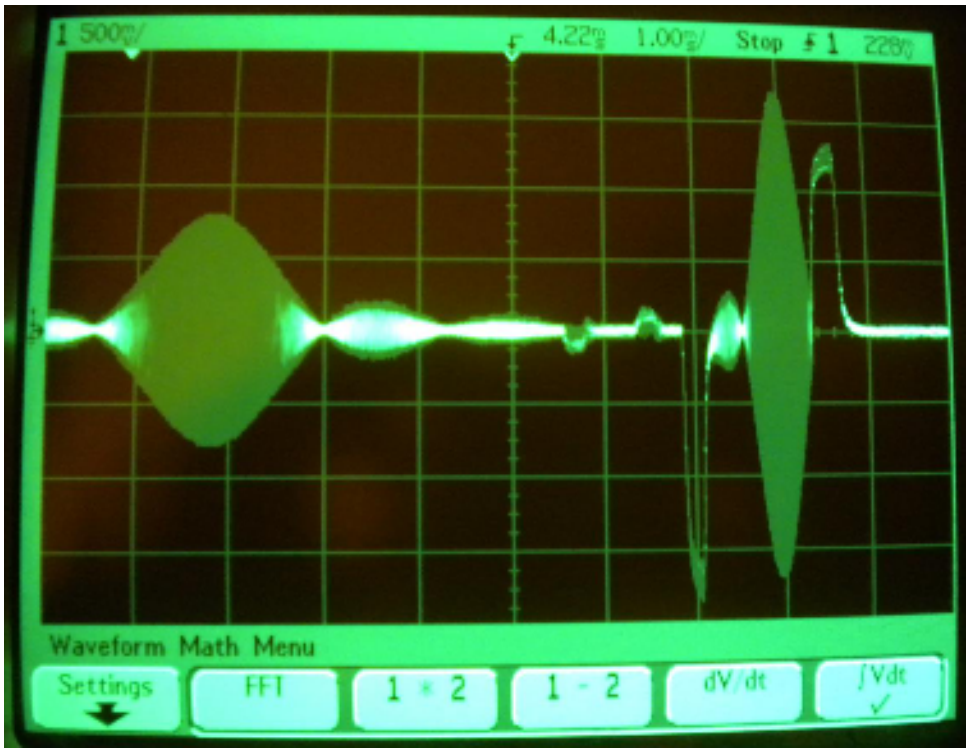

Figure 18: A more detailed presentation of the fat suppression RF pulse (on the left) and slice selection RF pulse in the middle of the slice selection gradient rise (negative) and fall (positive). The horizontal scale is 10 ms per square and vertical 500 mV per square.

The measurements performed further away from the isocentre, at about the position of a tall patients' knee (about 110 cm from the isocentre) and on the symmetry axis showed essentially the same dB/dt waveform. The amplitudes of the RF pulses had decreased by a factor of 10 and the gradient fields by a factor of about 20.

4.2 Artefact amplitude measurements

The measurements were performed using a DT9802 ADC with 50 kHz sampling frequency. Signal from the 10 first volumes of the EPI sequence was recorded for all positions and the seventh volume was analyzed.
Figure 19 shows the first 10 volumes of the EPI sequence recorded at 25 cm from the isocentre on the symmetry axis of the magnet. All the recordings had similar appearance. The seventh volume of the same signal is plotted in Figure 20. The plot of the seventh slice from the seventh volume is presented in Figure 21.

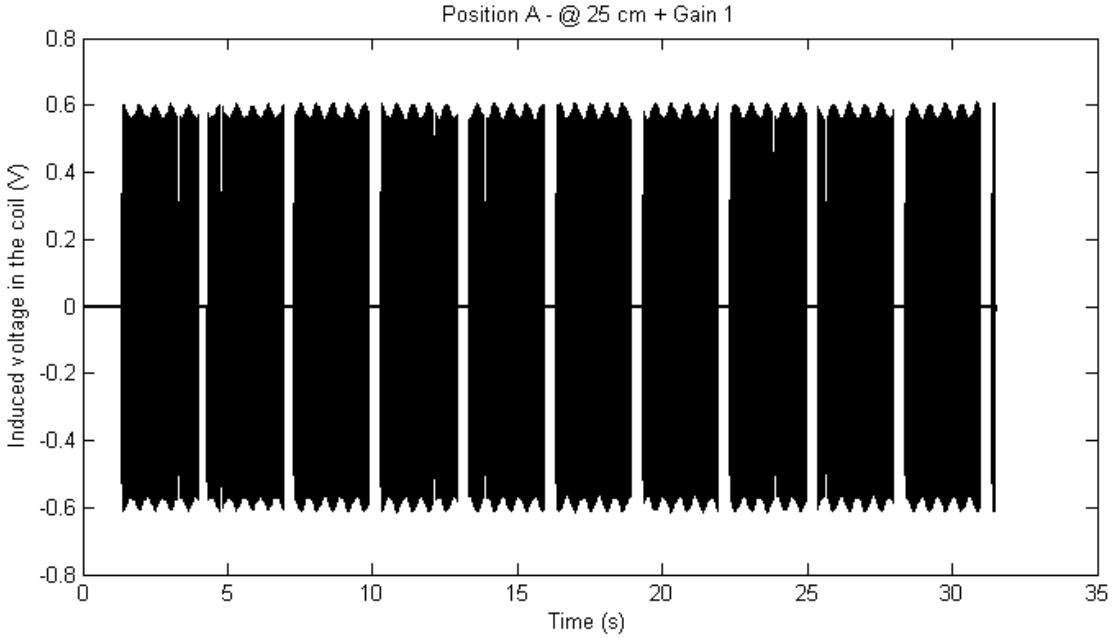

Figure 19: First ten volumes of the EPI sequence. On this figure, the whole signal is plotted. The coil was placed on the symmetry axis of the magnet, 25 cm from the isocentre.

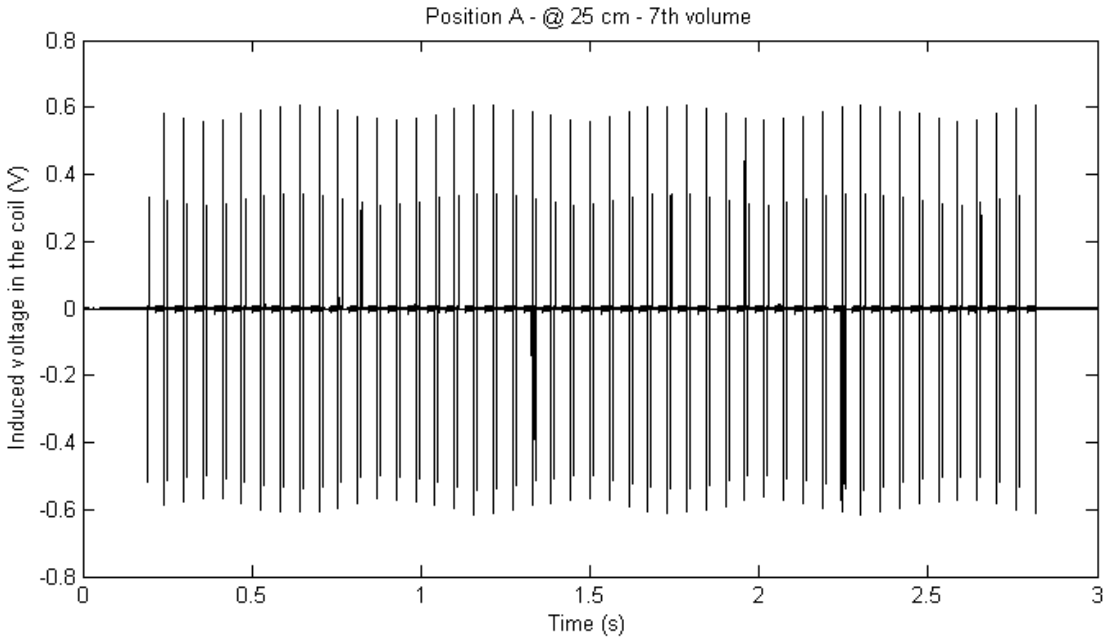

Figure 20: The seventh volume of the EPI sequence. The coil was placed on the symmetry axis of the magnet 25 cm from the isocentre.

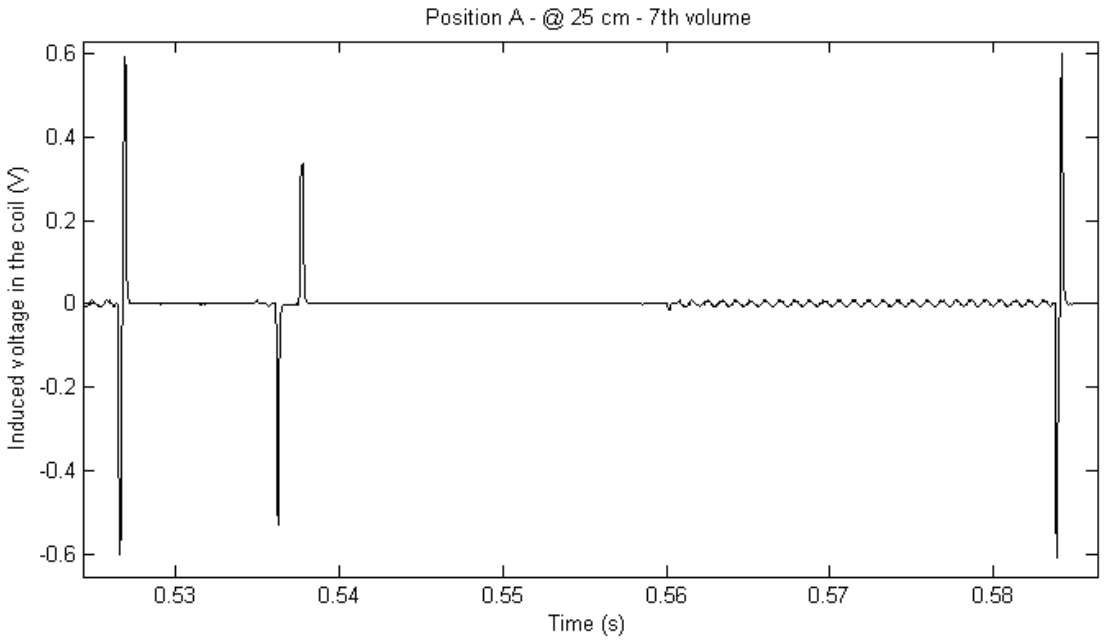

Figure 21: The seventh slice from the seventh volume of the EPI sequence at the distance of 25 cm from the isocentre.

Figure 22 presents the voltages induced by gradient switching measured on the symmetry axis of the magnet against the distance from the isocentre. The values from the document [11] were rescaled to fit the diagram.
The strongest peak values were measured at 25 cm from the isocentre. The slice selection gradient had also its strongest values at 25 cm. On the other hand, the readout part of the gradient had its strongest values at 50 cm. This might be due to slight misalignment of the coil or the fact that we were outside the linear region of the scanner.

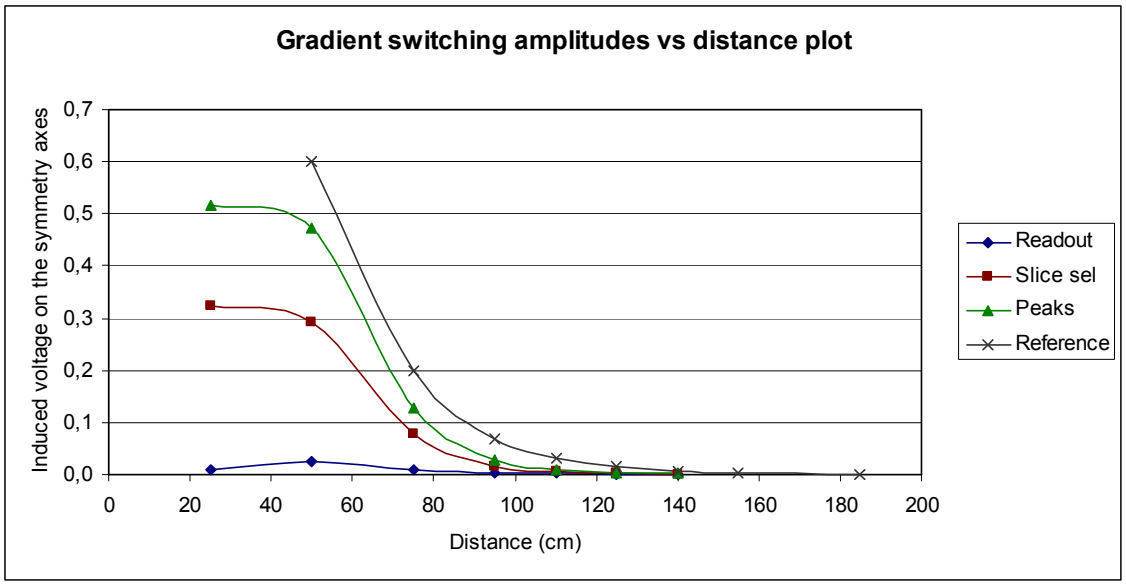

Figure 22: Gradient switching amplitude versus the distance from the isocentre plot. The reference data from document [11] was rescaled.

4.3 Effect of 430 kΩ resistor added in series with the coil

Figure 23 presents the seventh slice of the seventh volume of the Reference 4 signal and Figure 24 presents the seventh slice of the seventh volume measured at the same position at the rear side of the MR scanner with the 430 kΩ resistor added in series with the measuring coil.

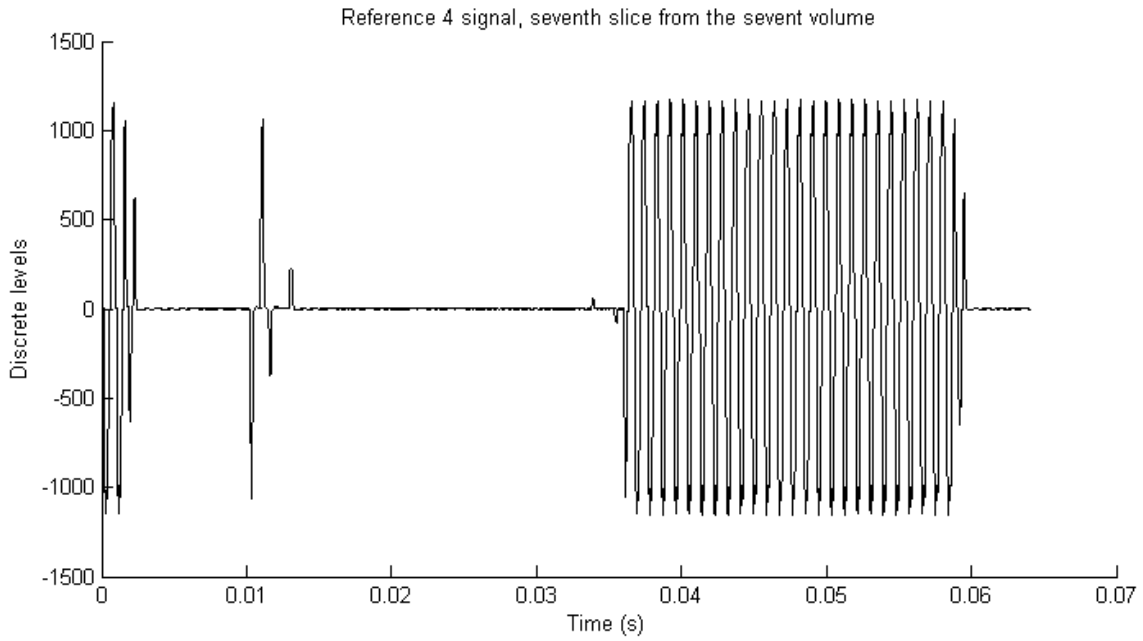

Figure 23: The seventh slice of the seventh volume of the Reference 4 signal.

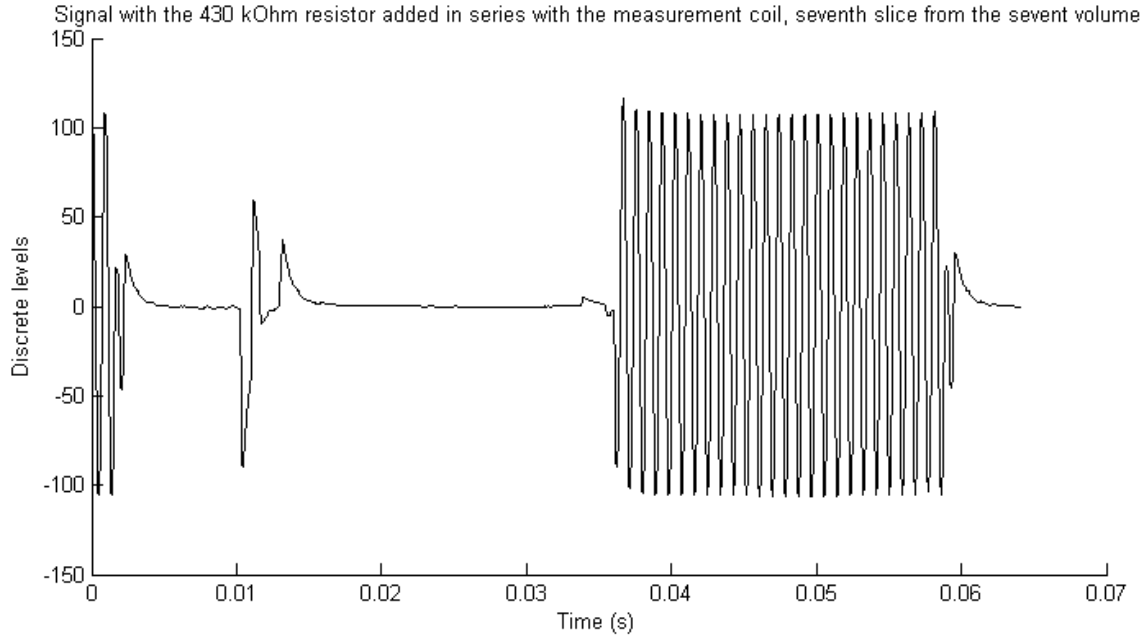

Figure 24: The seventh slice of the seventh volume measured with the 430 kΩ resistor added in series with the measuring coil at the same position as the Reference 4 signal.

Note the vertical scale difference of 10 times in Figure 23 and 24. The maximum amplitude difference was calculated to be 10,2 times. The added resistor has a smoothing effect on the signal.

4.4 Measurement results with the orthogonal coils

The cleanest measurement results with orthogonal coils from the rear side of the magnet were obtained with the coils placed as close to the tip of the head coil as possible. The gradient switching signals are presented in Figure 25 with black being the slice selection gradient (the normal of the measurement coil area was parallel to the symmetry axis of the magnet), red the frequency encoding gradient (horizontal direction orthogonal to the symmetry axis) and blue the phase encoding gradient (vertical direction). Figure 26 presents the same signals after integration (showing the magnetic field) and can be compared to Figure 9.

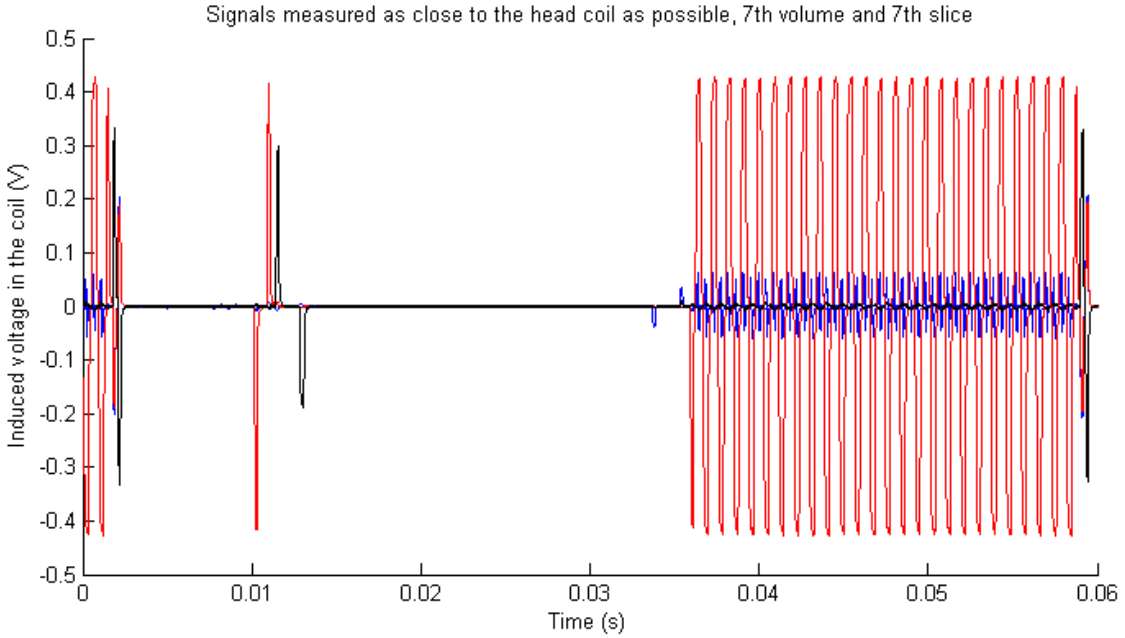

Figure 25: Gradient switching signals from the rear side of the magnet as close to the tip of the head coil as possible. Black is the slice selection, red the frequency encoding and blue the phase encoding gradient.

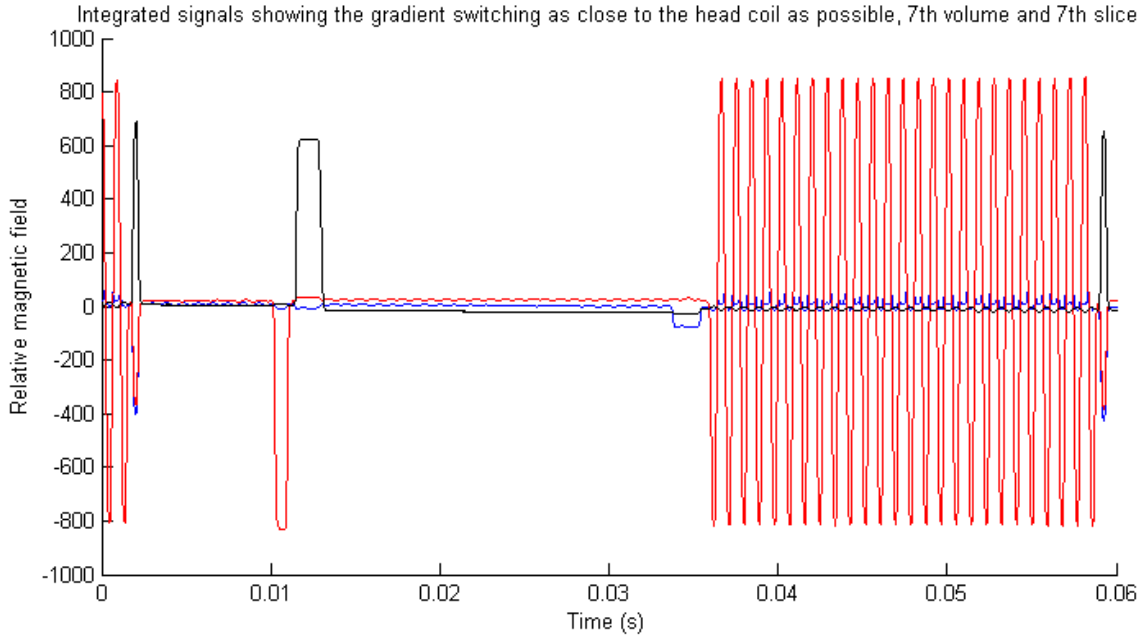

Figure 26: Gradient waveforms from the rear side of the magnet as close to the tip of the head coil as possible. Black is the slice selection, red the frequency encoding and blue the phase encoding gradient.

4.5 Frequency content of the signals

The spectral composition of the gradient switching signal from the front side of the magnet measured on the symmetry axis about 25 cm from the isocentre is presented in Figure 27 and with more details below 10kHz, in Figure 28.

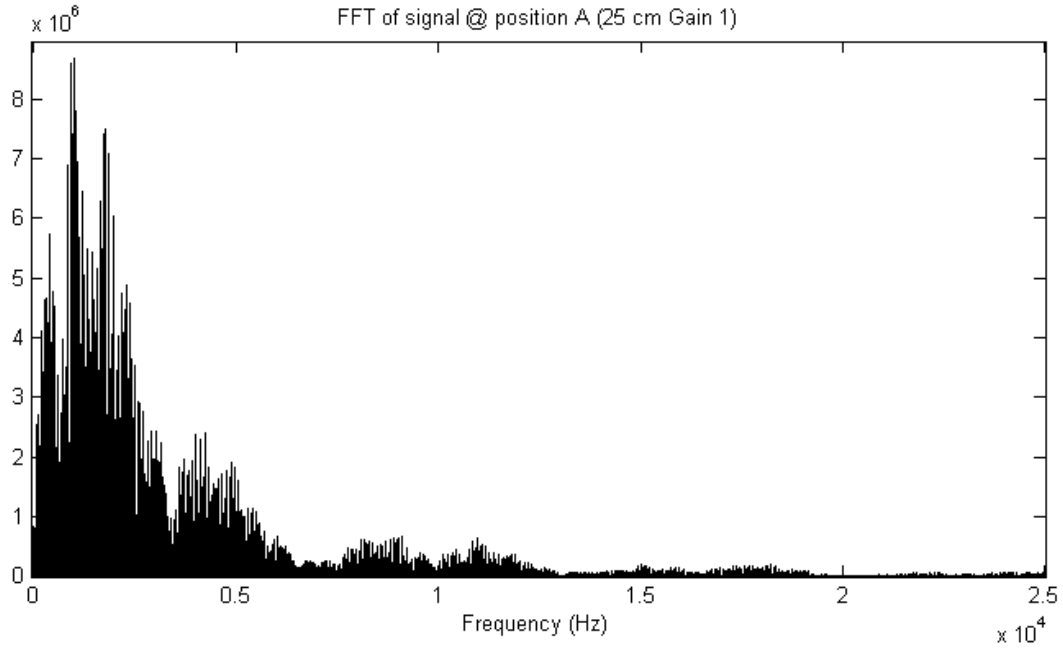

Figure 27: The spectral composition of the gradient switching signal recorded on the front side of the magnet, 25 cm from the isocentre and on the symmetry axis.

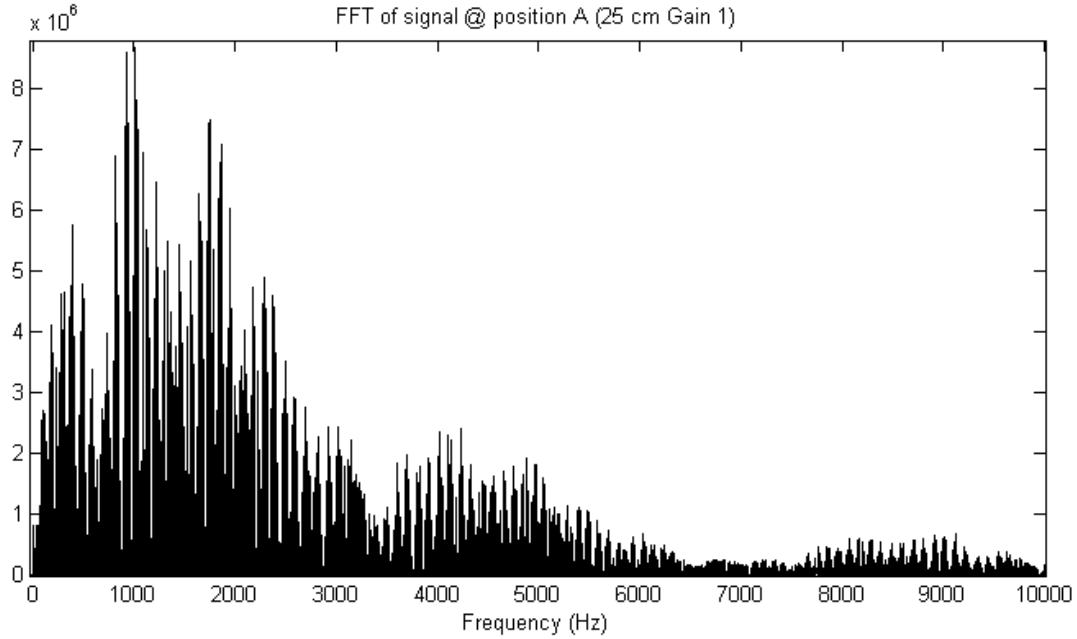

Figure 28: The spectral composition of the gradient switching signal recorded on the front side of the magnet, 25 cm from the isocentre and on the symmetry axis. Most of the information is below 10 kHz.

The gradient switching is composed of several different frequencies with the main power being around 1 kHz. Significant amount of the signal is below 10 kHz. Higher sampling frequencies are preferred as the purpose is to record the signal shape as precisely as possible.
The signal spectrum for microneurography measured outside MR environment is presented in Figure 29. It is filtered with a band-pass Butterworth filter similar to the one used in clinical practice. The filtering was performed in order to emphasise the frequency content of interest.

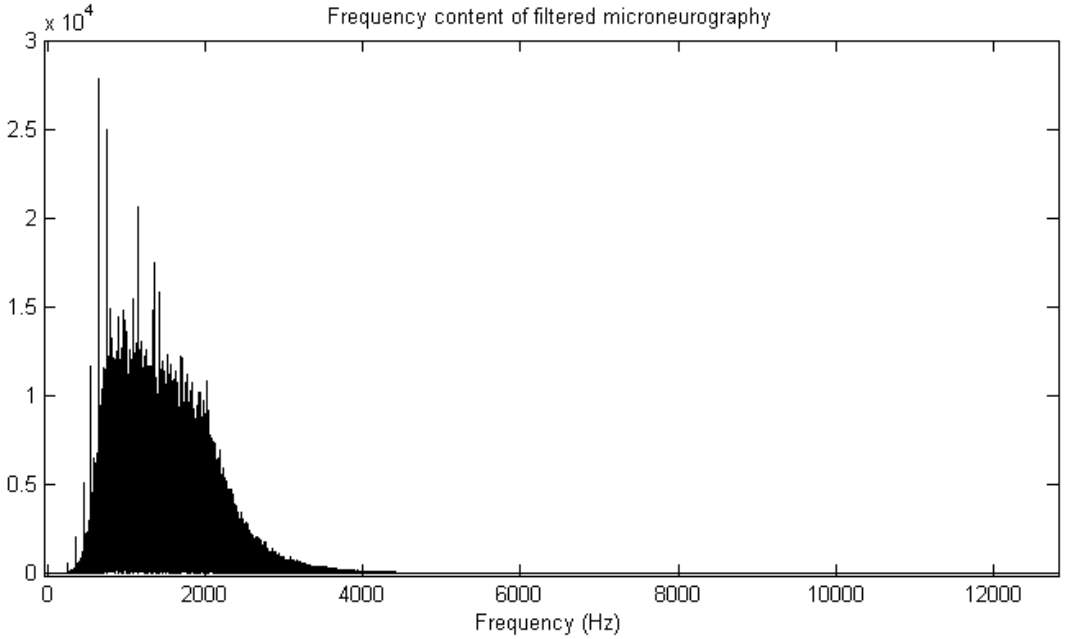

Figure 29: Frequency content of the microneurography signal after filtering, remaining frequencies are of interest. The filter used was a Butterworth bandpass filter with passband corner frequencies of 700 and 2000 Hz and stopband corner frequencies of 350 and 3000 Hz. The passband ripple was allowed to be 3dB and stopband attenuation of 20 dB.

The fundamental frequency of microneurography is around 1 kHz and differs slightly from subject to subject. Interesting information is between 700 and 2000 Hz. The filtering is usually done with a bandpass filter having corner frequencies between 700 and 2000 Hz in the passband and 350 and 3000 Hz in the stopband. The frequencies were chosen slightly narrower than presented in chapter 2.6 being the same as used in clinical practice at Sahlgrenska University Hospital. The ripple allowed in the passband was 3 dB and stopband attenuation was set to 20 dB.

4.6 Linear combination for artefact removal

The position and orientation of the coils for measuring reference signals and examined signals processed below is described in chapter 3.4. As previously, signals from the 10 first volumes of the EPI sequence were recorded and the seventh volumes analyzed. For all of the signals 1-4 the linear combination (explained in chapter 3.1) coefficients and corresponding signals were calculated, subtracted from the original signal, and the result (residual signal) was assessed with the help of reduction in the maximum absolute value and RMS value. Amplitude and RMS reduction was calculated by dividing the corresponding maximum values.
Table 3 presents the results of linear combination using two in-plane signals (upper and left) and the inner one (right) (Reference 1, 2 and 4) as the reference signals.

	Signal 1	Signal 2	Signal 3	Signal 4
Reference 1	0.0498	0.0337	0.0530	0.0150
Reference 2	-0.0471	-0.0335	-0.0028	0.0141
Reference 4	-0.0282	-0.0289	0.0111	0.0348
Maximum value of signal	59.73	52.06	55.07	55.07
Maximum value of result	12.26	9.81	9.99	6.60
Amplitude reduction	4.87	5.30	5.51	8.34
RMS of signal	26.28	23.26	6.20	21.44
RMS of result	1.37	1.49	1.04	0.94
RMS reduction	19.14	15.62	5.96	22.89

Table 3: Coefficients and linear combination evaluation parameters for the noise reduction with two in-plane signals and the inner one (Reference 1, 2 and 4). The maximum and RMS values are in discrete levels.

The variation of coefficients for different signals confirms that the gradient switching artefact has different waveforms depending on the position and orientation of the loop area. The maximum absolute values and RMS values of the artefact and residual signals are presented for illustrative purposes. The amplitude and RMS reductions describe the effectiveness of the method for different signals.
The best results from this experiment are for the fourth signal, having the RMS reduction of nearly 23 times and signal amplitude reduction of more than 8 times (which was also the best amplitude reduction for this set of signals and references). The seventh slice of the fourth signal is plotted in Figure 30 and its residual noise in Figure 31.

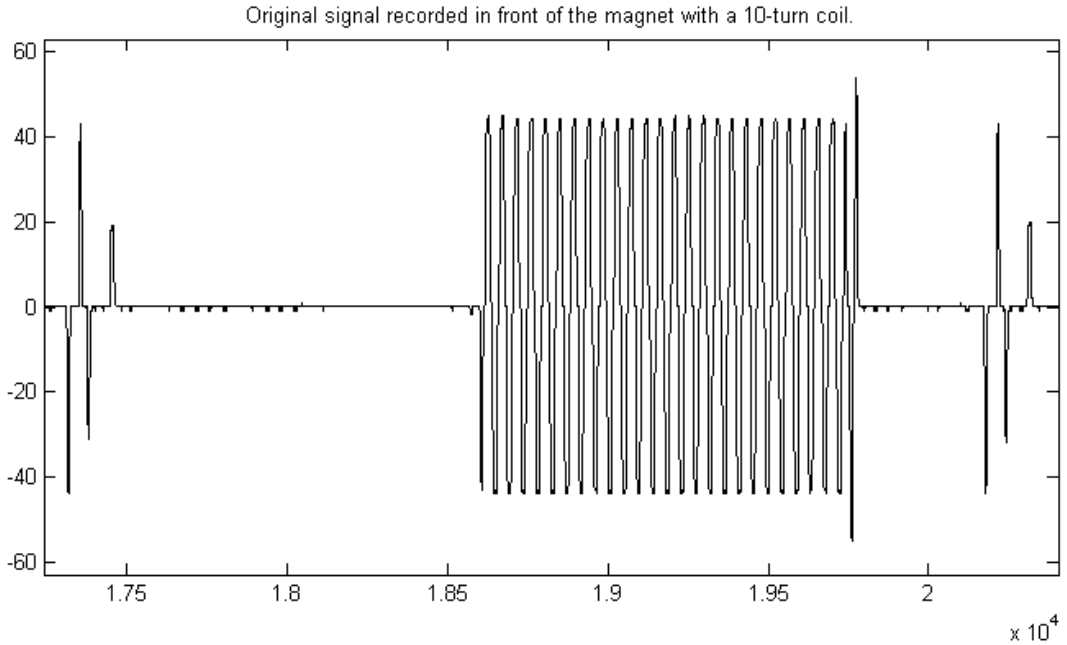

Figure 30: The seventh slice of signal 4. Since the signal shape is of interest, the vertical scale is left as recorded discrete levels and horizontal scale as sample numbers.

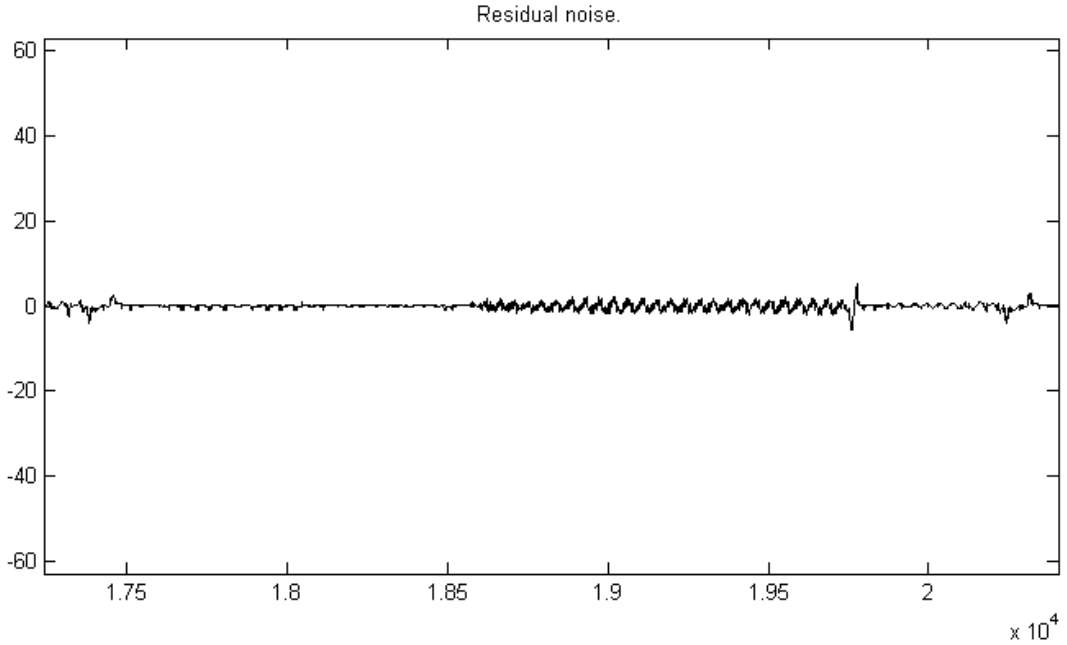

Figure 31: The residual noise of seventh slice of signal 4. The vertical and horizontal scales are presented with the same values as in Figure 30 (for better comparison).

The improvement by using all four reference signals for reconstruction instead of three was investigated and the results are presented in Table 4. The effect of using only three in-plane signals is presented in Table 5.

	Signal 1	Signal 2	Signal 3	Signal 4
Amplitude reduction	4.41	4.79	7.69	8.22
RMS reduction	19.69	18.03	6.65	33.25

Table 4: Amplitude and RMS reduction ratios when all four references (Reference 1, 2, 3 and 4) were used for calculating the linear combination for artefact removal. Only amplitude and RMS reduction ratios are presented here with the full table in the Appendix 1.

	Signal 1	Signal 2	Signal 3	Signal 4
Amplitude reduction	4.52	4.24	4.83	4.51
RMS reduction	13.01	9.96	4.75	9.59

Table 5: Amplitude and RMS reduction ratios when only the three in-plane references (Reference 1, 2 and 3) were used for calculating the linear combination for artefact removal. Only amplitude and RMS reduction ratios are presented here with the full table in the Appendix 1.

By comparing Table 3 and 4 it can be seen that using more reference signals improves the RMS reduction. On the other hand, the amplitude reduction improved only for signal 3. By close examination of the Reference 3 signal, it can be seen that it has quite strong noise present throughout the recording.
Using only the in-plane signals had significantly worse noise reduction (might be partly due to the noise on Reference 3).
The signal and residual noise from the best RMS reduction is presented in Figure 32. It was calculated for signal 4 using all four references from the rear side of the magnet. The best amplitude reduction can be seen on Figure 30 and 31.

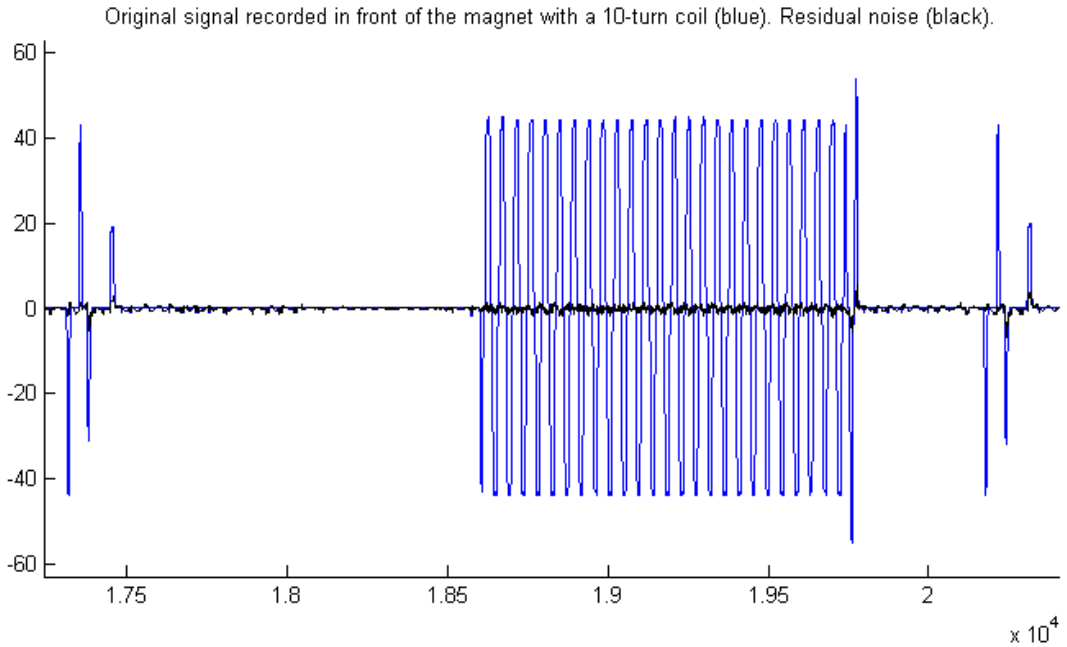

Figure 32: The original signal in blue and result in black for signal 4 using all four references from the rear side of the magnet. Since the signal shape is of interest, the vertical scale is left as recorded discrete levels and horizontal scale as sample numbers.

The method tries to minimize the RMS value of the residual signal. It can be seen from the results of signal 4 that using all four reference signals for the reconstructions increases the RMS reduction from 22.89 to 33.25 but the amplitude reduction decreases from 8.34 to 8.22 (compare Table 3 and 4).

4.7 Error produced by time misalignment

To investigate the error produced by time misalignment, a slightly time shifted copy of the signal was produced with Matlab command "interp1" (formula 13) and subtracted from the original signal. The maximum absolute amplitude of the difference was then divided by maximum absolute value of the original signal.
Table 6 presents the error (% of initial signal amplitude) produced by misalignment in time. Figure 33 shows the results for Reference 1 (recorded at the rear side of the scanner approximately 13 cm above the magnet symmetry axis (z-axis) and about 10 cm inside from the magnet end plane).

Misalignment (samples)	Misalignment (time, s)	Reference 1 (%)	Reference 2 (%)	Reference 4 (%)
0,0001	2,0E-09	0,0044	0,0043	0,0036
0,0003	6,0E-09	0,0132	0,0130	0,0109
0,0010	2,0E-08	0,0441	0,0432	0,0363
0,0030	6,0E-08	0,1324	0,1296	0,1090
0,0100	2,0E-07	0,4414	0,4320	0,3632
0,0300	6,0E-07	1,324	1,296	1,090
0,1000	2,0E-06	4,414	4,320	3,632
0,3000	6,0E-06	13,24	12,96	10,90
0,5000	1,0E-05	22,07	21,60	18,16

Table 6: Error produced by misalignment of the reference signals in time. Misalignment is expressed both in samples and in time. The worst case scenario misalignment is for Reference 1 by half of a sample producing an error with amplitude of 22% from the original signal amplitude.

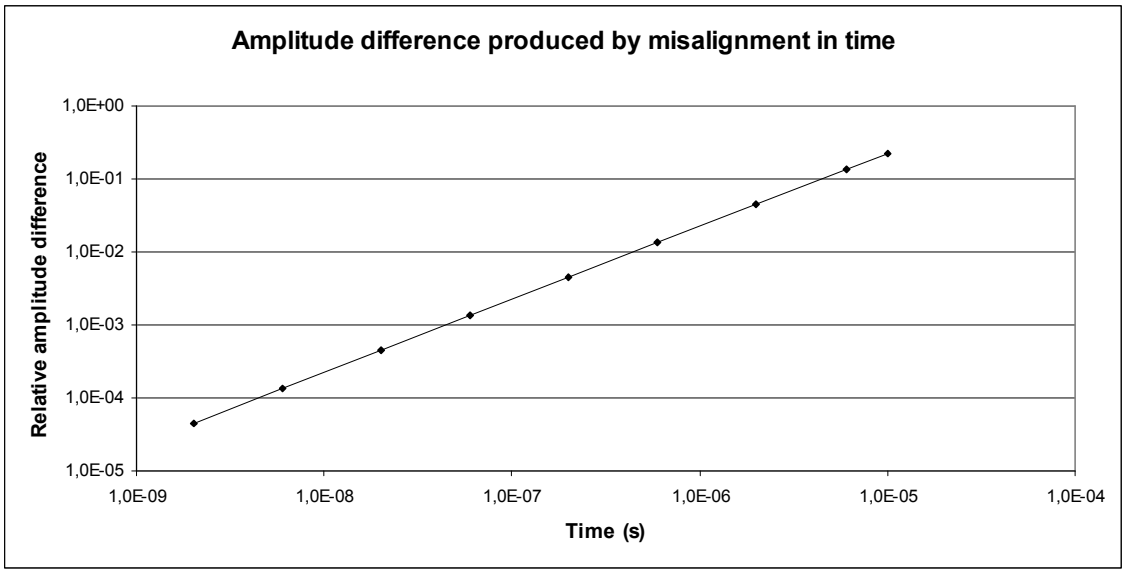

Figure 33: The relative amplitude difference depending on misalignment in time. The vertical axis shows the maximum value after subtraction of shifted copy from the original divided by the maximum value of the original. The horizontal axis shows the time misalignment between the original and shifted with the maximum value being shifted by half sample (worst case scenario).

Table 6 confirms the demand for ideal time alignment. Misalignment by half sample or 10 μs can produce an error in amplitude of up to 22 %. To get the possible error caused by misalignment down to 1%, the sampling frequency should be increased to a few MHz.

4.8 Testing linear combination on a synthesized signal

To see the capability of the linear combination method for ideally synchronized signals, a synthesized signal was produced consisting of a linear combination of the three reference signals. The same signals were used as references when performing the signal processing.
Reference 1, 2 and 4 were multiplied with three random numbers [3.1337, 0.1337, 5.3533] and the resulting signal processed. The synthesized signal is presented in Figure 34 and the result after removing the artefact in Figure 35. Table 7 presents the linear combination coefficients, amplitude and RMS reductions, as for the previous calculations.

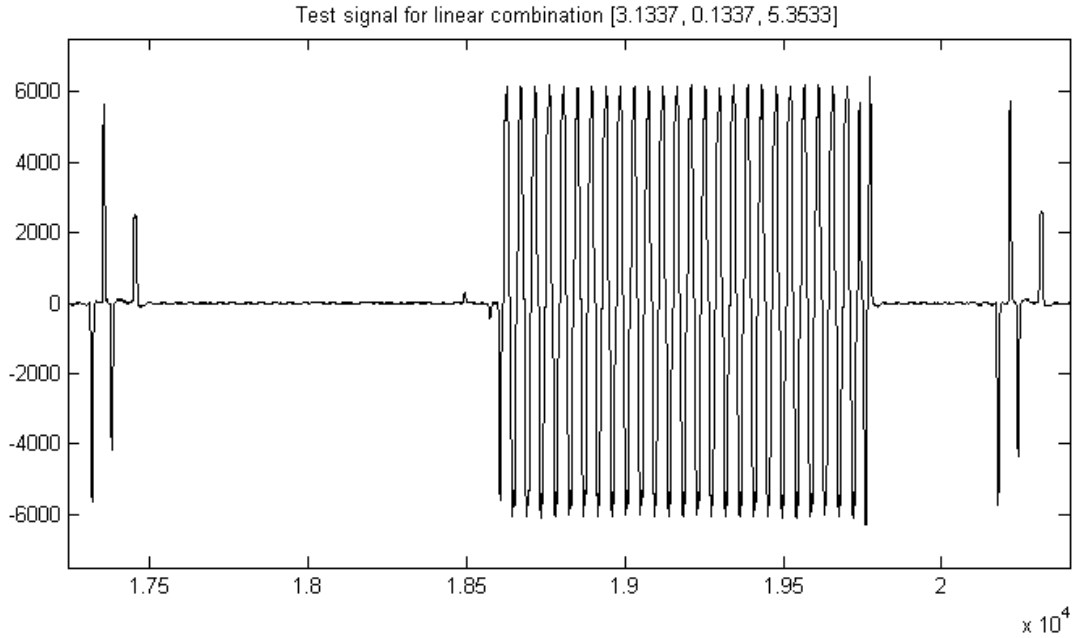

Figure 34: The synthesized signal consisting of [3.1337, 0.1337, 5.3533] times Reference 1, 2 and 4. Since the signal shape is of interest, the vertical scale is left as recorded discrete levels and horizontal scale as sample numbers

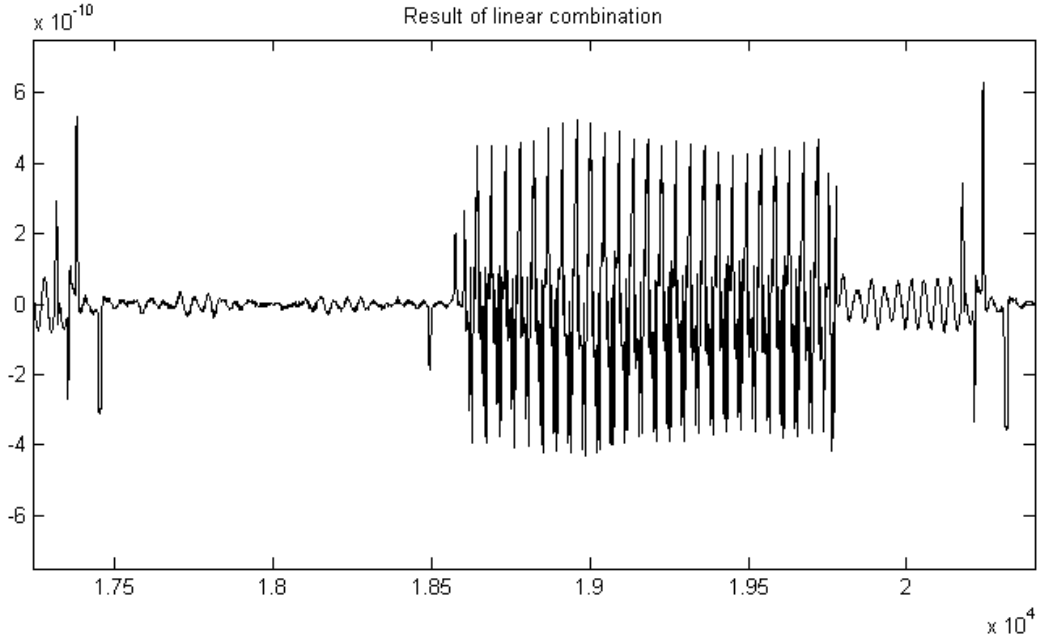

Figure 35: Result after calculating the linear combination and subtracting the signals. Note the 10^{13} difference on the vertical scale. Since the signal shape is of interest, the vertical scale is left as recorded discrete levels and horizontal scale as sample numbers

	Synthesized signal
Reference 1 Reference 2 Reference 4	3.1337 0.1337 5.3533
Maximum value of signal	6.95 e+003
Maximum value of result	7.61 e-010
Amplitude reduction	9.13 e+012
RMS of signal	2.80 e+003
RMS of result	1.46 e-010
RMS reduction	1.92 e+013

Table 7: Coefficients and linear combination evaluation parameters of the noise reduction for the synthesized signal. The maximum and RMS values are in discrete levels. The maximum and RMS values are in discrete levels.

The signal reduction by the factor of 10^{13} should be sufficient to prove that the linear combination method is working. The remaining error is probably due to rounding errors produced by Matlab.

4.9 Testing the effect of linear combination on added periodic signals

Continuous sine and cosine signals from the same frequency range as the gradient switching were added to the synthesized signal in order to see their effect on the linear combination method and *vica versa*. The microneurography signal measured outside the MR environment was also tested. The synthesized artefact signal composed of a linear combination of three reference signals (Reference 1, 2 and 4) multiplied with coefficients [3.1337, 0.1337, 5.3533]. The magnitude of the added signal, representing microneurography and being the signal of interest, was about 100 times less than the synthesized signal.

Two sets of sine and cosine signals were added. The first one had approximately 76% of amplitude of 950 Hz cosine and 24% of 2200 Hz sine signal. The second had approximately 63% of amplitude of 975 Hz cosine and 37% of 1200 Hz sine signal. The microneurography signal was added *ad hoc*. The maximum absolute and RMS values with the magnitude and RMS reduction ratios are presented in Table 8.

The maximum values and RMS values were calculated using formulas (9) and (10). The final noise signal was obtained by subtracting the cleaned signal (the one gone through the artefact removal process) from the original signal of interest. The magnitudes were calculated by dividing the corresponding values.

Signal of interest:	cos: 950 Hz, sin: 2,2 kHz	cos: 975 Hz sin: 1,2 kHz	Micro-neurography
Reference 1 coefficient for artefact removal	3.1323	3.1330	3.1337
Reference 2 coefficient for artefact removal	0.1343	0.1335	0.1337
Reference 4 coefficient for artefact removal	5.3529	5.3535	5.3533
Maximum value of synthesized signal with added signal of interest (**initial signal**)	6.988e+03	6.955e+03	6.959e+03
Maximum value of **signal of interest**	58.8389	58.8711	0.0031
Maximum value of result after subtraction of linear combination (**cleaned signal**)	59.3651	59.3666	0.0031
Maximum difference between the signal of interest and the cleaned signal (**final noise**)	1.0859	0.7666	5.4256e-06
Magnitude of final noise on the initial signal (synthesized + signal of interest)	1.554e-04	1.102e-04	7.797e-10
Magnitude of final noise on the cleaned signal	0.0183	0.0129	0.0018
RMS of synthesized signal with added signal of interest (initial signal)	2.801e+03	2.801e+03	2.800e+03
RMS of signal of interest	33.2114	30.4949	0.0011
RMS of cleaned signal	33.2112	30.4949	0.0011
RMS of difference between signal of interest and cleaned signal	0.0912	0.0692	1.3618e-06
RMS of final noise on the initial signal	3.257e-05	2.472e-05	4.863e-10
RMS of final noise on the cleaned signal	0.0027	0.0023	0.0012

Table 8: The results after adding the signals of interest to the synthesized signal composing of [3.1337, 0.1337, 5.3533] times the reference signals. All results have dimensions in discrete levels or ratios.

The results describe the effect of adding signals from the same frequency range as the gradient shifting on the linear combination method (change in the synthesized signal coefficients) and the effect that linear combination has on the signals of interest (the final noise on the cleaned signal).
Adding periodic signals from the same frequency range as the gradient shifting results in a decrease of accuracy of the linear combination method. The synthesized signal consisted of [3.1337, 0.1337, 5.3533] times the reference signals but the method calculated the coefficients as [3.1323, 0.1343, 5.3529] and [3.1330, 0.1335, 5.3535]. The small difference in coefficients also indicates that the signal of interest has been affected by the calculations. The RMS of the signal of interest was influenced by 0.2 - 0.3 % and the amplitude was changed 1 - 2 %. The microneurography signal was affected even less by the linear combination method. The resulting noise is caused by insufficient artefact removal.
In order to see the difference between the processed and original microneurography, the final post-processing was performed as in clinical practice. Both signals were band-pass filtered, rectified and moving average was calculated. The results are presented in Figure 36 with the original microneurography in blue and the one gone though the artefact removal process in black.

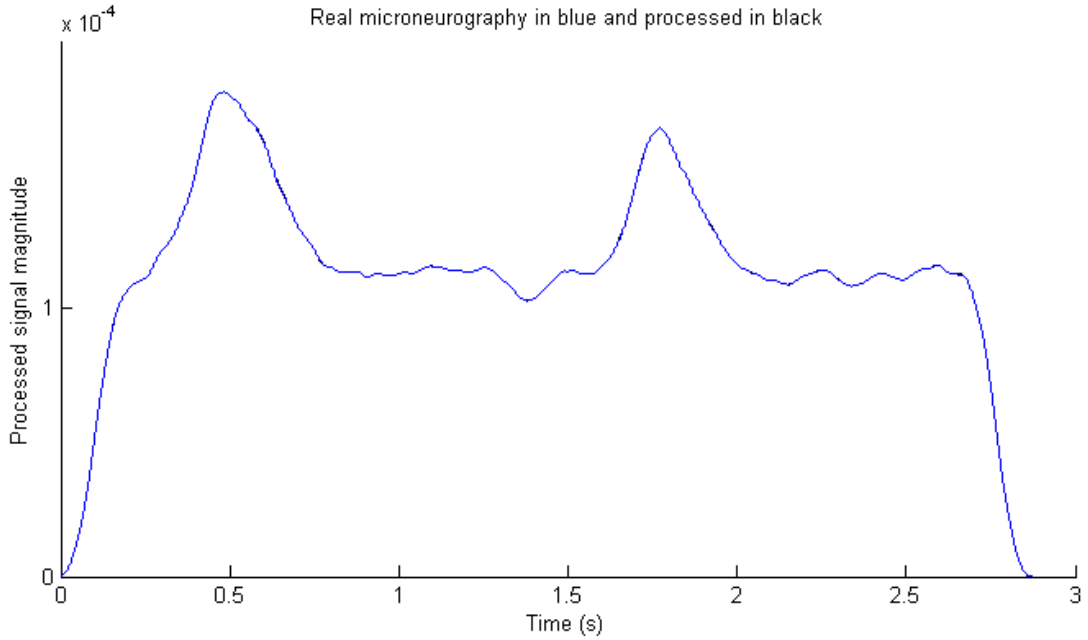

Figure 36: The results of the final post-processing as done in clinical practice for the original microneurography signal in blue and the one gone though the artefact removal process in black . Since the signals overlap, the black one is not visible.

4.10 Effect of filtering prior to linear combination

The effect of low-pass and high-pass filtering of the references and signals prior to calculating the linear combination was investigated with Butterworth filters.
Since the signals were not measured simultaneously, a slight misalignment of maximum half a sample, or 10 μs might still be present between the recordings. Low-pass filtering is expected to reduce the effect of misalignment in the final result.
Low-pass Butterworth filtering was performed with three different edge frequencies. Passband corner frequencies were chosen to be 6500, 10000 and 13000 Hz. Stopband corner frequencies were chosen respectively as 10000, 13000 and 20000 Hz. For all filters, passband ripple was set to 3 dB and stopband attenuation to 20 dB. The results for the first filter (6500 and 10000 Hz as corner frequencies) are shown in Table 9.

	Signal 1	Signal 2	Signal 3	Signal 4
Amplitude reduction	5.8666	5.5127	6.0378	8.5938
RMS reduction	20.9528	16.7825	6.1992	24.4545

Table 9: Calculation results for Butterworth low-pass filter using passband corner frequency of 6500 Hz, stopband corner frequency of 10 kHz, passband ripple of 3 Db and stopband attenuation of 20 dB. Only amplitude and RMS reduction ratios are presented here with the full table in the Appendix 2.

High-pass filtering was performed with Butterworth filter having the passband corner frequencies of 700, 500 and 300 Hz. Stopband corner frequency was chosen to be 50 Hz for all cases. Passband ripple was set to 3 dB and stopband attenuation to 20 dB, as before. The results for the filter with 500 Hz passband corner frequency are presented in Table 10.

	Signal 1	Signal 2	Signal 3	Signal 4
Amplitude reduction	5.0756	6.2305	5.7876	8.0480
RMS reduction	18.5863	15.1611	5.8902	22.5312

Table 10: Calculation results for Butterworth high-pass filter using passband corner frequency of 500 Hz, stopband corner frequency of 50 Hz, passband ripple of 3 Db and stopband attenuation of 20 dB. The maximum and RMS values are in discrete levels. Only amplitude and RMS reduction ratios are presented here with the full table in the Appendix 2.

Low-pass filtering had a positive effect on the method by removing the high frequency noise present in the recordings. Both RMS and amplitude reduction on the residual signal improved for all signals with tested corner frequencies. Since the corner frequencies are outside the microneurography signal region, it should not have an effect on the signal of interest and therefore can be suggested to be used in the final set-up.
On the other hand, high-pass filtering resulted in decreased efficiency with the passband corner frequencies of 500 and 700 Hz. Only the test with 300 Hz corner frequency slightly improved the results.
The tables with the results from the other filters are presented in Appendix 2 - Effect of filtering prior to linear combination.

4.11 Linear combination with time-shifted copies of the reference signals

To investigate the effect of possible time misalignment, a test was made with slightly time-shifted copies of the reference signals. The orthogonal signals measured with 100 kHz sampling frequency at the rear side of the magnet as close to the head coil and symmetry axis as possible were used as reference signals. The reference signals and artefact signals measured at the knee position were synchronized manually.
First, the linear combination coefficients with corresponding artefact signal amplitude and RMS reduction was calculated for each of the signals (Table 11). Then, two time shifted copies of the reference signals were created with the Matlab command "interp1", one shifted by 0.1 sample (1 μs) to the left (before) and the other by 0.1 sample to the right (later). The linear combination was calculated using the three original reference signals plus the six time-shifted reference signals. The results were analyzed as previously and are presented in Table 12.

Knee site	Horizontal (freq)	Vertical (phase)	z-direction (slice)
Reference vertical	-0.0123	0.0841	-0.0065
Reference horizontal	-0.1792	0.0622	-0.0300
Reference z-direction	0.1359	-0.0809	-0.1083
Maximum value of signal	174.6773	117.6997	69.3010
Maximum value of result	23.7510	6.0986	11.3919
Amplitude reduction	7.3545	19.2995	6.0834
RMS of signal	73.0036	26.8344	12.7845
RMS of result	4.4953	1.4115	1.3314
RMS reduction	16.2400	19.0108	9.6022

Table 11: Linear combination coefficients and noise reduction parameters when only the three original signals recorded at the rear side of the magnet as close to the head coil as possible were used for reconstructions. The maximum and RMS values are in discrete levels.

Knee site	Horizontal (freq)	Vertical (phase)	z-direction (slice)
Sum of Ref vertical	-0.0142	0.0847	-0.0062
Sum of Ref horizontal	-0.1790	0.0620	-0.0300
Sum of Ref z-direction	0.1360	-0.0810	-0.1082
Amplitude reduction	13.7017	19.6363	13.4188
RMS reduction	30.5652	20.4380	12.8493

Table 12: The sum of original and shifted reference coefficients and amplitude and RMS reduction ratios for the test which used both the original reference signals and the time-shifted copies for artefact removal. Full table can be found in Appendix 3.

There is quite a remarkable improvement in the reduction of artefact signal when the time-shifted copies of the reference signals are included in the calculations. Especially for the horizontal signal which is in the frequency encoding gradient direction that has most power. The RMS reduction of the artefact has increased nearly 1.9 times.
The linear combination coefficients (or the sum of coefficients in one direction) remain nearly the same for nine references as it was for three references.
The horizontal signal measured in front of the magnet at the approximate knee position is presented for illustrative purposes on Figure 37. The result after artefact removal using both the original references and time-shifted copies is presented in Figure 38.

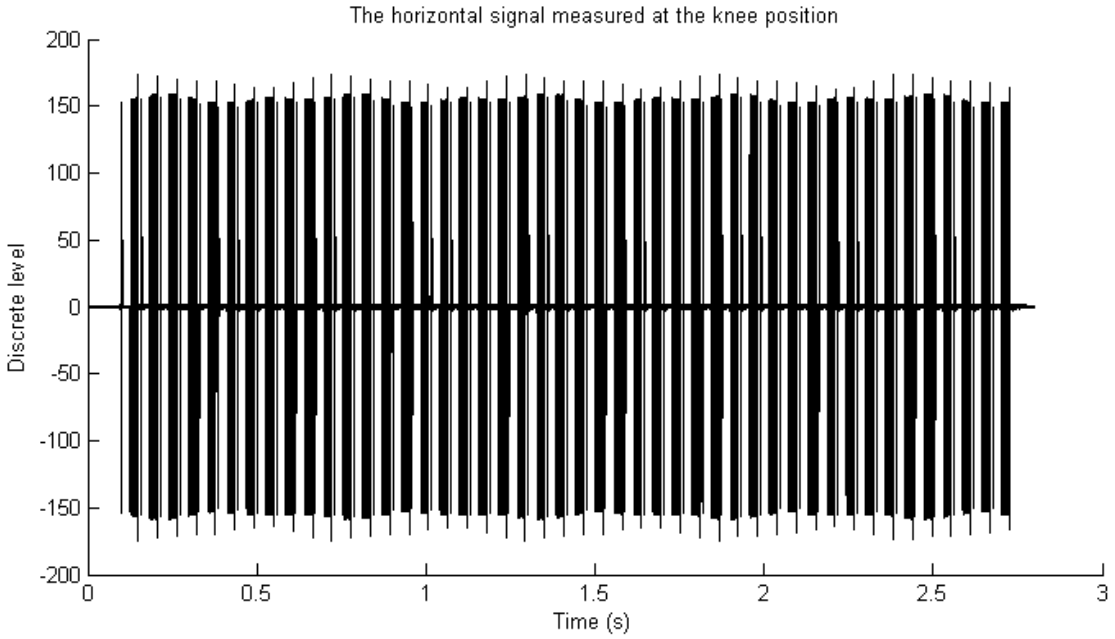

Figure 37: The frequency encoding gradient signal measured at the approximate knee position in front of the magnet.

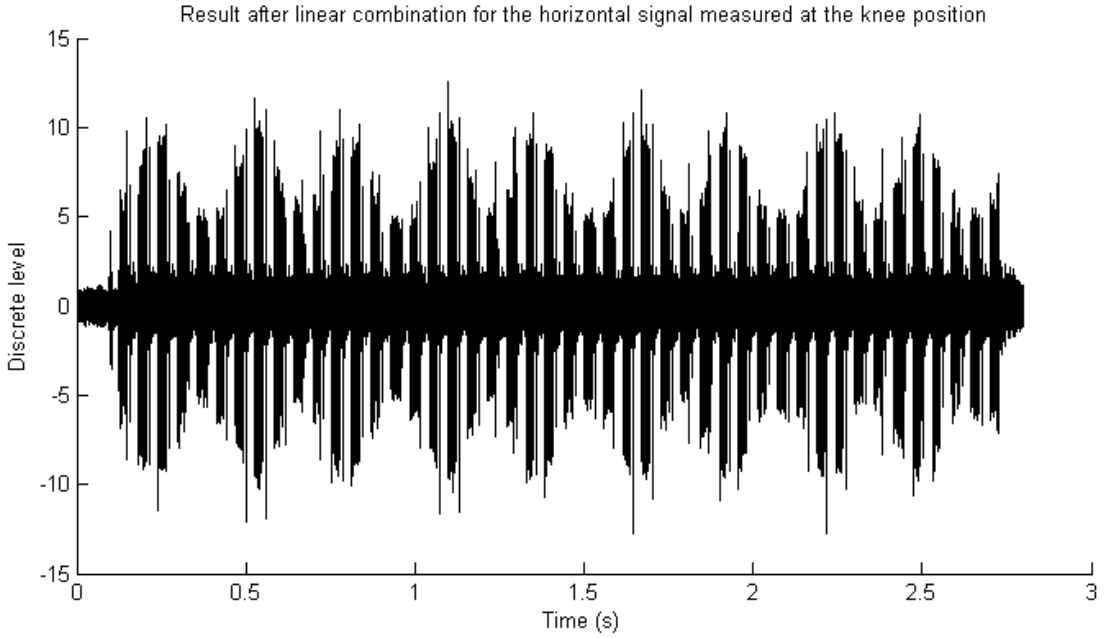

Figure 38: Result after the artefact removal for the frequency encoding gradient presented in Figure 37. Both original references from the measurement set close to the head coil and time-shifted copies were used for the artefact removal.

Since the vertical signal seemed to be slightly shifted in time by about half a sample compared to the other signals and references, a test was made where it was shifted by one sample and the same reconstructions procedure was repeated. The results are presented in Table 13.

Knee site vertical signal	Synchronization 1		Synchronization 2	
	Three references	Nine references	Three references	Nine references
Amplitude reduction	19.2995	19.6363	4.4875	19.5859
RMS reduction	19.0108	20.4380	7.7176	21.2337

Table 13: Amplitude and RMS reduction ratios for the vertical signal before and after shifting it by one sample in time. Synchronization 1 is the same one used for previous results in Table 11 and 12. Full table can be found in Appendix 3.

The effect of shifting the artefact signal by one sample in time results in remarkably different results for artefact removal. The RMS reduction differs almost 2.5 times. On the other hand, including the time-shifted copies of the reference signals, the other time position has slightly better results. The correct time synchronization is somewhere between the two samples.

4.12 Reconstructions with real microneurography added to the measured signals

To see how the current set-up would work in a real life situation, an artefact signal was synthesized from the three orthogonal signals measured at the approximate knee position with the 100 kHz sampling frequency. The microneurography signal recorded outside the MR environment was added and the linear combination was calculated for artefact removal. The orthogonal signals measured at the rear side of the magnet as close to the head coil and symmetry axis as possible were used as reference signals.
The approximate area of a microelectrode loop is about 2 dm^2. To have a fairly bad estimation, the artefact signals were rescaled to correspond to 1,8 dm^2 each. Nine reference signals were used for artefact removal.
The part of the microneurography signal used in the experiment was chosen to have two bursts over the reconstruction period. The peak-to-peak voltage of the upsampled microneurography was 23,60 µV. It must be noted that the microneurography signal had quite strong 50 Hz noise and after filtering with a Butterwoth bandpass filter with corner frequencies of 700 and 2000 Hz and stopband corner frequencies of 350 and 3000 Hz (passband ripple 3 dB, stopband attenuation 20 dB), the peak-to-peak voltage had decreased to 12,48 µV.
The peak-to-peak voltage of synthesized artefact signal was 266,61 mV. This means that the peak-to-peak amplitude ratio between the microneurography signal and the gradient switching artefact is

$$\frac{23{,}60\,\mu V}{266{,}61 mV} = 8{,}85 \cdot 10^{-5}$$

The SNR was calculated with formula 14 as

$$SNR = \left(\frac{RMS(microneurography)}{RMS(artefact)} \right) = \left(9{,}54 \cdot 10^{-5}\right)^2 = 9{,}10 \cdot 10^{-9}$$

Linear combination coefficients were calculated for the synthesized signal, which was later used as the supplementary signal, and for the synthesized signal with the added microneurography. The maximum amplitude and RMS reductions were evaluated as for the previous calculations. The resulting signals along with the original microneurography signal were filtered and moving average was calculated with a normalized triangular convolution kernel.
The result of filtering of the original microneurography (black) and artefact removed signal (blue) is presented in Figure 39. The result after calculating the moving average of rectified filtered microneurography (black) and rectified filtered artefact removed signal (blue) is presented in Figure 40. It can be seen that the moving average of the artefact removed signal follows the activity of the residual noise after artefact removal process.
The supplementary signal is expected to have similar residual noise activity areas as the artefact removed signal and can be used for additional artefact removal. Since the same synthesized signal was used as the supplementary signal, subtracting the filtered, rectified and leaky integrated results of the two should give an estimation of the microneurography signal as the result. The result is presented on Figure 41.
It can be seen that the artefact removal process has to be significantly improved and can not be used for estimating the bursting activity. Additionally, in a real life situation the supplementary signal would differ more from the gradient switching artefact picked up by the microelectrode loop.

The linear combination coefficients and artefact removal parameters for the signal with artefact, supplementary signal and original microneurography signal is presented in Table 14.

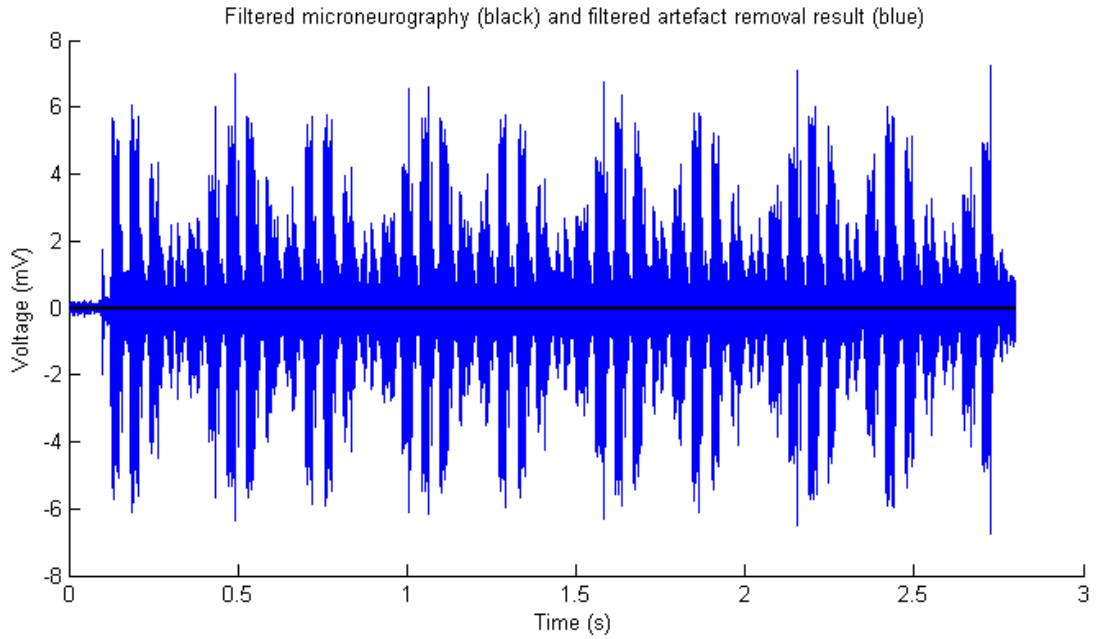

Figure 39: Original microneurography signal after filtering (black) and filtered result after artefact removal (blue). Note that the peak-to-peak difference of the signals is nearly 10^5 ($8{,}92*10^4$) times, hence the black line for the microneurography signal appears as zero .

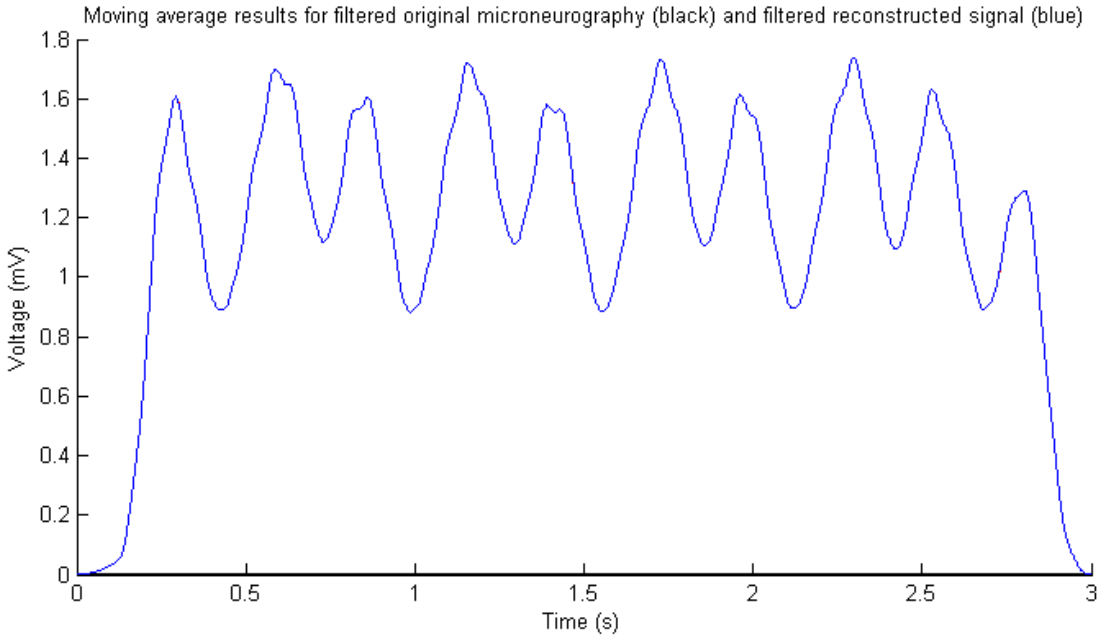

Figure 40: Moving average of rectified and filtered original microneurography signal (black) and rectified and filtered artefact removed signal (blue). Note the maximum amplitude difference of $5{,}0*10^4$, meaning that the microneurography is not visible.

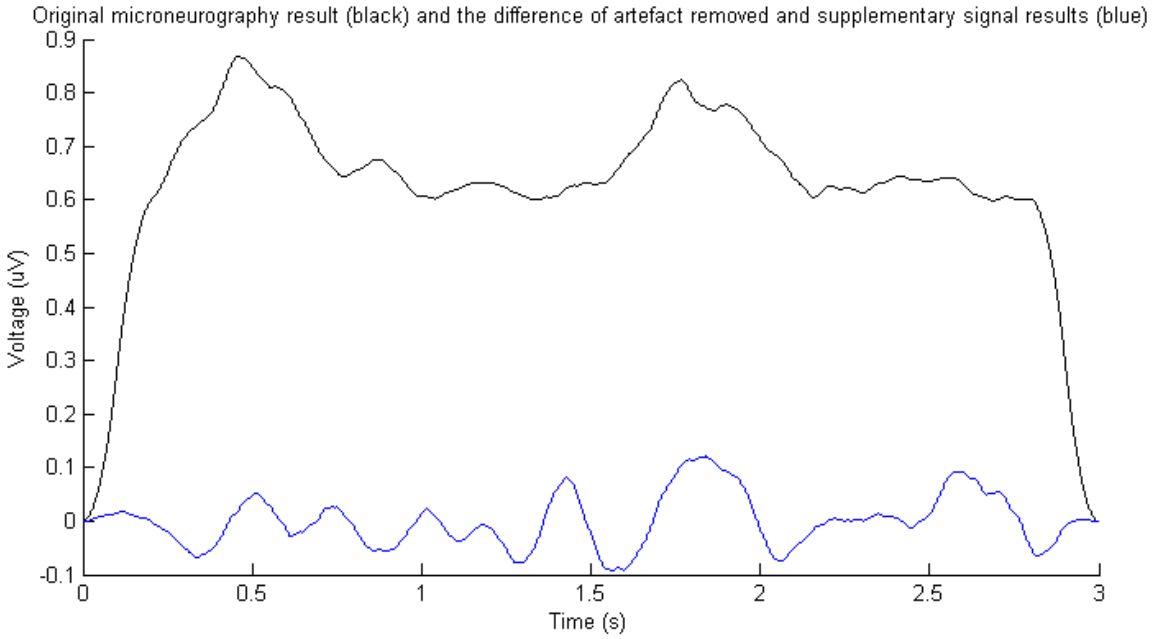

Figure 41: Moving average of rectified and filtered original microneurography signal (black) and subtracted difference of signal with artefact and supplementary signal (blue). Note the vertical scale being in µV.

	Synthesized signal	Microneurography signal	Microneurography signal + artefact
Maximum value of signal	133.7199 (mV)	0.0149 (mV)	133.7185 (mV)
Amplitude reduction by least squares fit	13.5212		13.5120
RMS of signal	56.8208 (mV)	0.0054 (mV)	56.8208 (mV)
RMS reduction by least squares fit	26.2673		26.2672
Peak-to-peak amplitude ratio			8.8503e-005
SNR			9.1030e-009

Table 14: Comparison of synthesized signal (used also as supplementary signal), original microneurography signal and the microneurography signal with the added gradient switching artefact (synthesized signal). Additional entries can be found in Appendix 4.

In order to see how much the method has to be improved, the microneurography signal was amplified and the artefact removal process repeated. The results for the microneurography amplification of 10, 100, 1000 and 10000 times is presented in Table 15.

The “peak-to-peak amplitude ratio after artefact removal”, “peak-to-peak amplitude ratio after leaky integrator” and “Square of RMS ratio after leaky integrator” have been calculated by comparing the corresponding values for original microneurography signal and artefact removed result signal. For ideal artefact removal the values would be equal to 1.

Microneurography signal amplification and peak-to-peak voltage	1 23,60 µV	10 236,0 µV	10^2 2,360 mV	10^3 23,60 mV	10^4 236,0 mV
Maximum absolute value of signal with artefact, (mV)	133.72	133.71	133.58	141.82	255.43
Amplitude reduction by least squares fit	13.51	13.43	12.66	7.45	1.72
RMS of signal, (mV)	56.82	56.82	56.82	57.08	78.51
RMS reduction by least squares fit	26.27	26.26	25.48	9.78	1.45
Peak-to-peak amplitude ratio for signal and artefact	8.85e-05	8.85e-04	0.0089	0.0885	0.8850
SNR for signal with artefact	9.103e-09	9.103e-07	9.103e-05	0.0091	0.9103
Peak-to-peak amplitude ratio after artefact removal	8.921e-04	0.0089	0.0913	0.7462	0.9984
Peak-to-peak amplitude ratio after leaky integrator	4.992e-04	0.0050	0.0498	0.4295	0.9809
Square of RMS ratio after leaky integrator	2.683e-07	2.682e-05	0.0027	0.2011	0.9556

Table 15: Results after artefact removal by least squares fit. Different amplification of the microneurography signal was used prior to adding the artefact signal. Full table can be found in Appendix 4. The peak-to-peak amplitude ratio after artefact removal, peak-to-peak amplitude ratio after leaky integrator and SNR after leaky integrator have been calculated by comparing original microneurography result and artefact removed result.

All images looked the same for the 10 times amplification case. Only the vertical scale in Figure 41 was 10 times higher.
Moving average of the 100/1000/10000 times amplified (and filtered and rectified) microneurography signal is presented in Figure 42/44/46 in black and the artefact removed signal in the same image in blue. Figure 43/45/47 presents the same microneurography signal in black and the difference between artefact removed and supplementary signal (after filtering and rectifying) in blue.

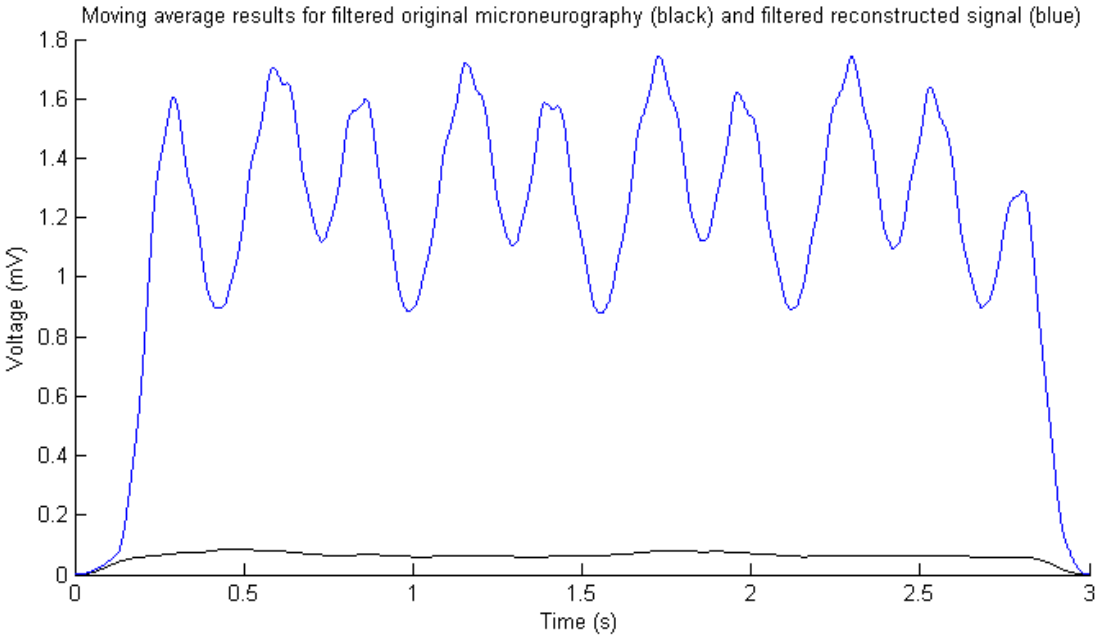

Figure 42: Moving average of the 100 times amplified (and filtered and rectified) microneurography signal (black) and the artefact removed signal (blue).

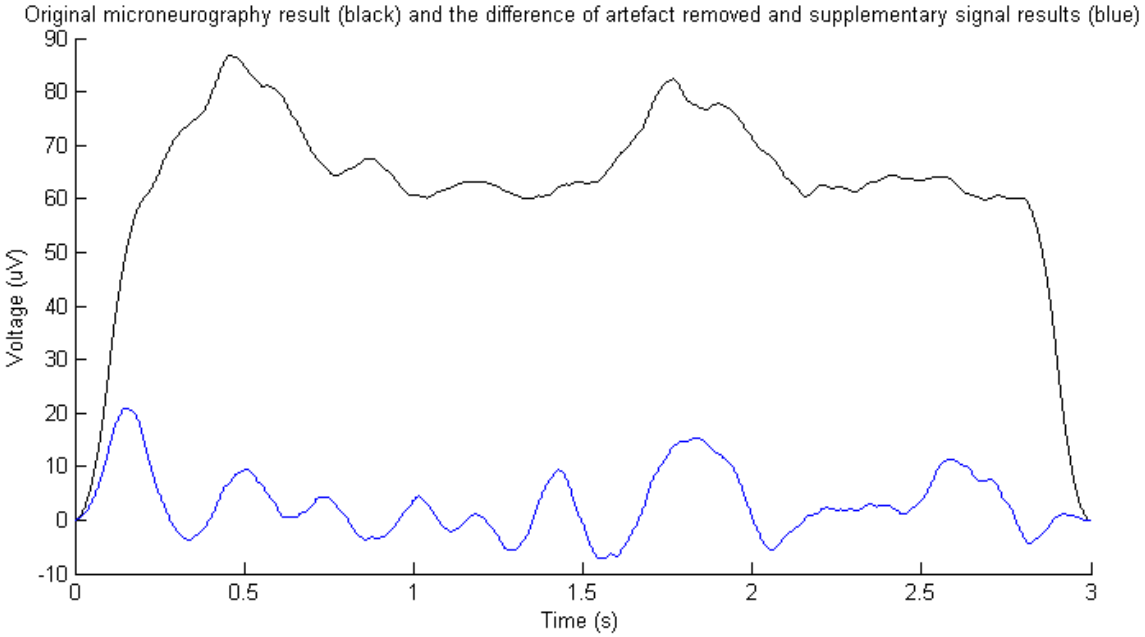

Figure 43: Moving average of the 100 times amplified (and filtered and rectified) microneurography signal (black) and subtracted difference of signal with artefact and supplementary signal (blue). Note the vertical scale being in µV.

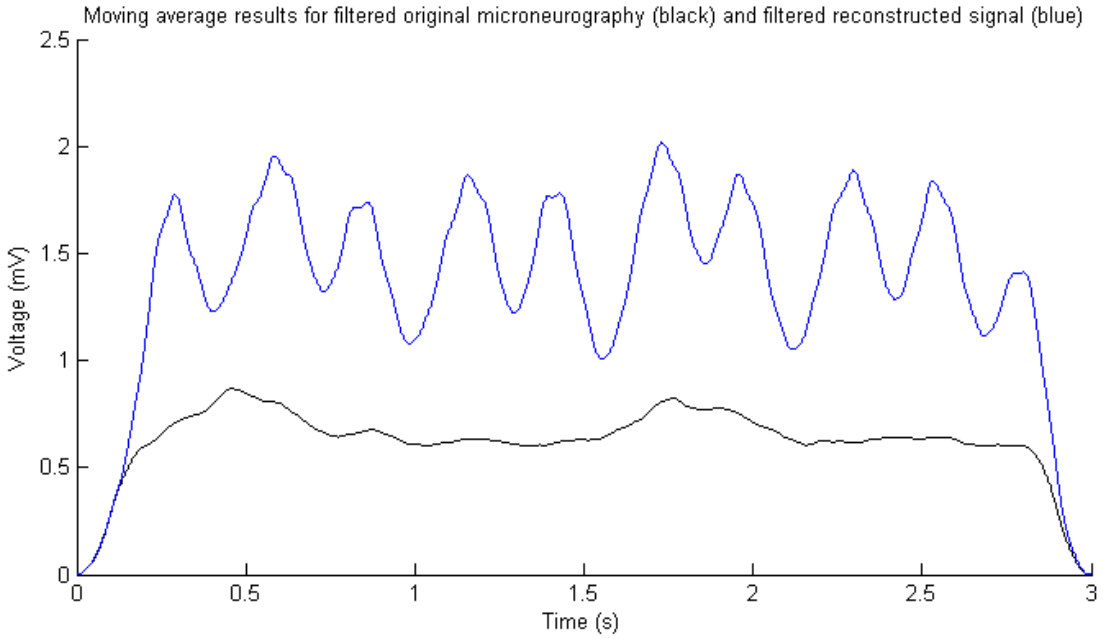

Figure 44: Moving average of the 1000 times amplified (and filtered and rectified) microneurography signal (black) and the artefact removed signal (blue).

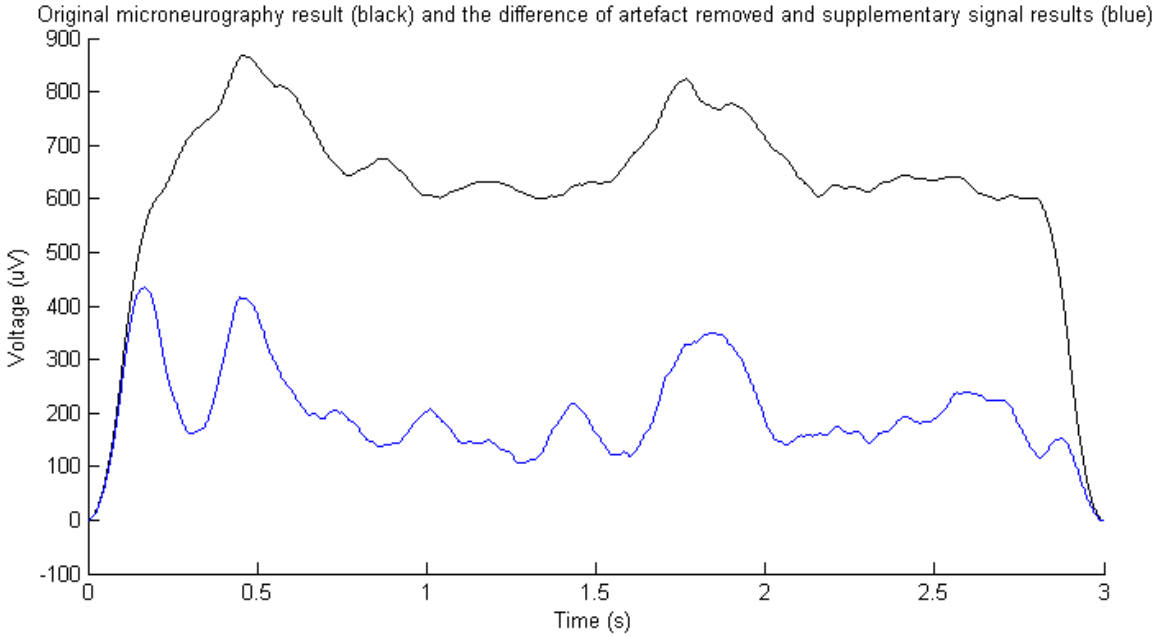

Figure 45: Moving average of the 1000 times amplified (and filtered and rectified) microneurography signal (black) and subtracted difference of signal with artefact and supplementary signal (blue). Note the vertical scale being in µV.

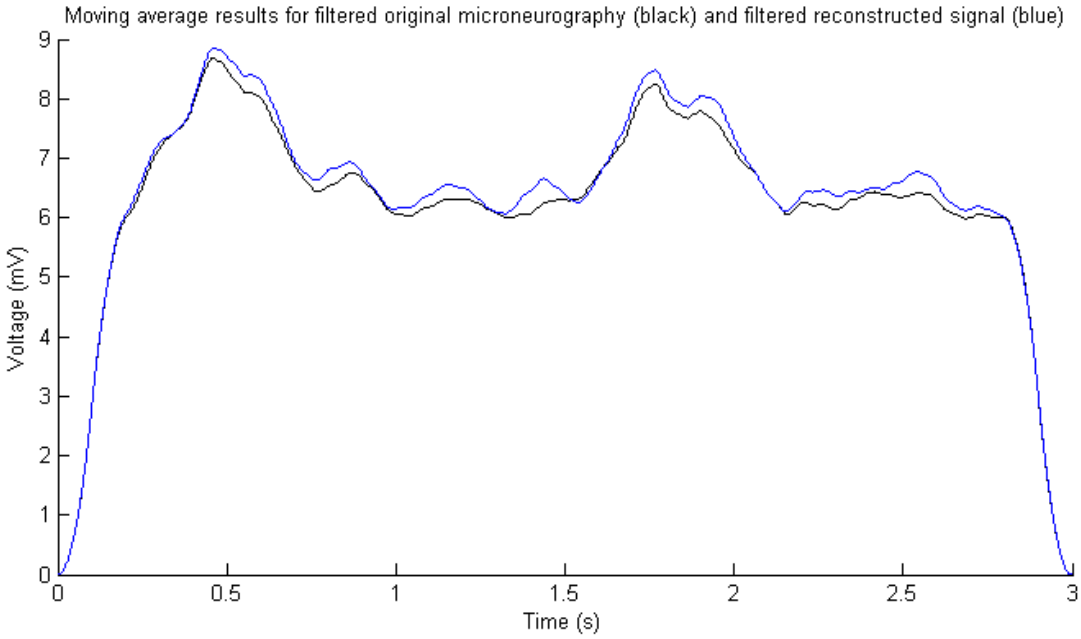

Figure 46: Moving average of the 10000 times amplified (and filtered and rectified) microneurography signal (black) and the artefact removed signal (blue).

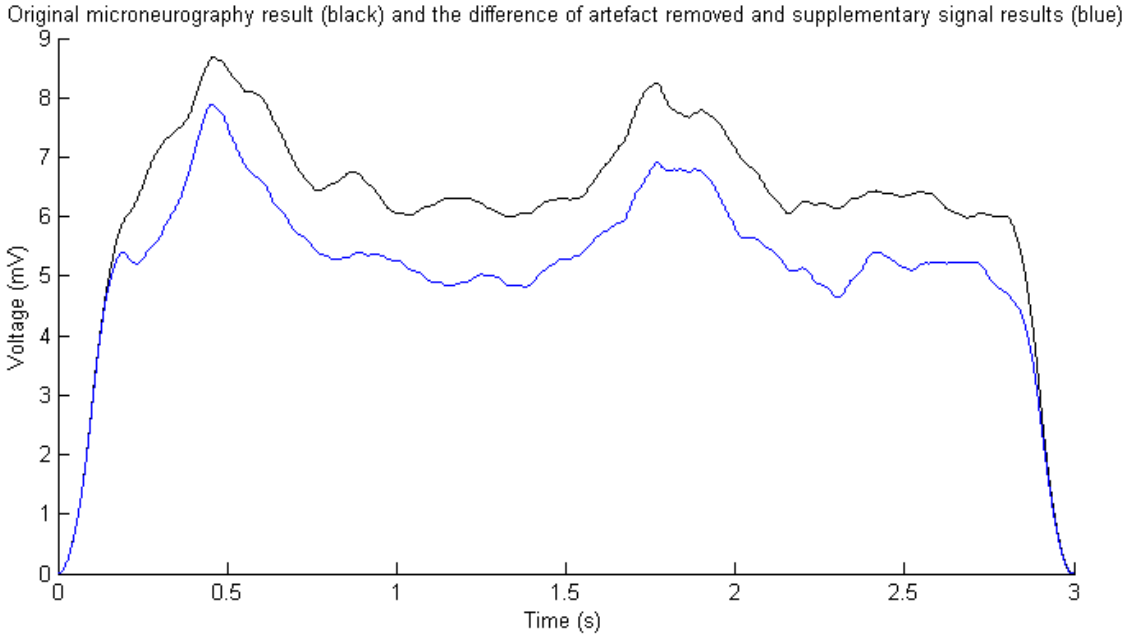

Figure 47: Moving average of the 10000 times amplified (and filtered and rectified) microneurography signal (black) and subtracted difference of signal with artefact and supplementary signal (blue). Note the vertical scale being in mV.

5. Discussions

5.1 Concept

When performing microneurography measurements simultaneously with MR scanning, the unavoidable microelectrode loop will also pick up signals from the gradient switching. Since the frequency ranges of microneurography signal and the gradient switching artefact overlap, filtering of the artefact signal can not be used. Instead, by recording the microneurography signal with the gradient switching artefact and the gradient switching itself as precisely as possible, the artefact can be estimated and subtracted form the contaminated microneurography signal.
There are three orthogonal gradient fields which mean at least three reference signals must be recorded in properly selected positions. The positions have to be chosen so that the independent portion of each gradient field is maximized for at least one of the reference signals. If so, the signals can be treated as reference signals for calculating the linear combination for artefact removal. A fourth reference loop can be added following the electrode loop as closely as possible in order to use it for the remaining noise removal after subtracting the linear combination result.
The reason for using reference measurements instead of modelling the gradient fields is that the aim was to keep the set-up and signal processing as simple as possible. This includes the fact that it should be applicable for all pulse sequences and timing parameters. Modelling would limit the method to a specific pulse sequence and timing parameters and would have to be recalculated for each modification of the pulse sequence. Furthermore, the modelled fields must still be subtracted from the microneurography measurement and the coefficients will change from subject to subject since the size and orientation of the electrode loop will be different for each patient.

5.2 Recordings

The first measurements performed in the MR environment demonstrated that the gradient switching waveforms can be recorded in detail. With sufficient prior knowledge about the pulse sequence, the different gradient directions (i.e. slice, phase and frequency encoding) can be distinguished. The RF pulses are recognizable and correspond to the simulated sequence used for the experiments (compare Figure 9 and Figure 17). The maximum voltage induced in the coils was in the same order as theoretically calculated.
The closest distance of the measurement coil from the isocentre of the magnet was chosen to be 25 cm because the scanners maximum field of view is 50 cm (extending 25 cm to the both sides from the isocentre). At 25 cm the coil would be on the edge of the linear region but still outside the imaging field. The vicinity of the linear region should minimize the signal to only one gradient direction (i.e. the slice selection gradient since the measurements were also performed on the symmetry axis). The motivation for being outside the imaging field is to minimize the possibility for image artefacts.
Figures 17 and 21 have contamination from phase and frequency encoding gradients due to a small possible misalignment of the measurement coil.
Analyzing and plotting the seventh volume for all results was chosen *ad hoc*. The first two volumes are always scanned in order to achieve magnetic (eddy current) steady state and no imaging is performed. Therefore it was chosen to be one of the following volumes.

The coils and electronics used for recording the signals were not calibrated since the main purpose was to measure the shape of the waveform rather than measure absolute amplitudes in milliteslas per second (mT/s). Therefore it was necessary to rescale the data from the reference document [11] to match the amplitudes in Figure 22. The strongest peak values were measured at about 25 cm from the isocentre of the magnet. The normal of the measuring coil was set parallel with the symmetry axis of the magnet and therefore the slice selection gradient, having the same direction, was dominant on the recordings. The contamination from phase and frequency encoding gradients, being perpendicular to this direction, was due to a small misalignment of the measurement coil and the fact that the measurements further away from the isocentre were performed outside the linear region of the magnet. This is probably the reason why the readout part of the gradient has an increase in amplitude at 50 cm (see the gradient switching amplitude *versus* distance from the isocentre plot in Figure 22). Since the gradient mode was set to maximum and peripheral nerve stimulation (PNS) mode was set to "high" for all of the recordings, all gradients (i.e. slice, phase and frequency encoding) are expected to have comparably high values and it is sufficient to record only one. If the exact values were to be compared, the measurement coils must be calibrated and measurements performed in all three directions.

Since the measurement results on the symmetry axis of the magnet were similar to the results in [11], it can be used as a starting point for the future studies about the electromagnetic fields of this MR scanner. The document also demonstrated the strongest voltage induced by the gradient switching being at the distance of approximately 35-40 cm from the isocentre of the magnet close to the magnet covers. This is where the gradient coils are located. Further away from the isocentre the amplitudes drop off quite rapidly.

The 3D distribution of the static field in [11] corresponded to the datasheet provided by Philips, static field gradient and gradient fields (for four pulse sequences, including the EPI sequence) were also measured. Additionally, the RF distribution was described with E and H-fields. The document can be recommended as an introduction for the future studies, but has to be validated for each application.

All measurements were performed one after another with the scanner running the same pulse sequence. The signals were synchronized manually by aligning the time of the spoiler gradient pulse. The spoiler gradient pulses were used for synchronization due to being present in all three orthogonal directions at the same time.

Correlation calculated on the whole signal lengths was also tried for synchronisation. Since the signals measured in different positions in the scanner bore have different positive and negative slopes, depending on the gradient direction, it did not provide correct results. For example, signals measured on different sides of the bore have the same polarity for the slice selection gradient but different polarity for the frequency encoding gradient. Additionally, orthogonal gradients have different activity areas. Correlation should be possible to use for fine synchronisation on shorter intervals of the signals.

Figure 25 plots the gradient switching dB/dt waveforms measured on the rear side of the magnet with three orthogonal coils and Figure 26 plots the actual gradient waveforms that can be compared to the stimulated waveforms presented in Figure 9. The measured waveforms closely resemble the simulated waveforms one demonstrating the accuracy of the measurements.

One of the main ideas was that it should be possible to use reference signals recorded at the rear side of the scanner for gradient artefact removal. During a microneurography study many other physiological parameters are recorded as well, e.g. blood pressure, ECG, breathing, skin conductivity (sweating), etc. This results in many other devices

being connected to the patient and recording the reference signals on the rear side would minimize the possibility of accidental errors.

5.3 Signal processing

Least squares fit for calculating the linear combination coefficients was first used for artefact signals measured in front of the magnet and reference signals measured at the rear of the magnet. The positions of the coils are described on Figure 12 and 14.
The variation of coefficients confirms that different positioning and orientation of the electrode loop will pick up different proportions of each gradient field. Since the signals were not measured simultaneously, a slight misalignment of up to half a sample, or 10 μs was still likely present between the recordings even after manual synchronization.
The results presented in Figures 30 and 31 give the proof of principle that the linear combination method works, but has to be significantly improved before it can be applied to microneurography measurements during MR scanning. Since the gradient switching signal picked up by the electrode loop is expected to be in the order of several hundred mV and the microneurography is in the order of a few tens of μV, the gradient artefact reduction by a factor of 10^{-5} – 10^{-6} is required. The strongest errors are at the edges of steep gradient changes. This means that a very precise synchronization is crucial.
Using more reference signals for reconstructing the artefact waveform improves the RMS reduction (compare Table 3 and 4). On the other hand, amplitude reduction improved only for signal 3. Close examination of the Reference 3 waveform reveals it having a quite strong ringing noise present throughout the recording. The origin of this noise was believed to be from the mechanical vibration of the scanner covers transferred to the coil.
Calculating the dot (scalar) product of the artefact signal and the reference signals to obtain the coefficients for artefact removal was also tried. The problem was that the recordings had a strong common mode (all reference recordings were performed with the normal of the coil being parallel to the symmetry axis). The method worked well on some parts of the signals but at the parts with the common mode the error increased. Least squares fitting was used in the following experiments.
To confirm the significance of proper time alignment, a test was made where a slightly time-shifted copy of the signal was subtracted from itself. The time shifting was achieved by creating additional time points by linear interpolation between the original samples. The results demonstrated that the misalignment of half a sample can cause an error of more than 20 % of the initial amplitude. This means that if a gradient artefact reduction of 10^{-5} in amplitude is required, the time misalignment must be less than 0,0003 samples or 5 ns (Figure 33). This will require either a sampling frequency of about 200 MHz or corresponding upsampling for proper time alignment of the signals. Consequently, simultaneous recordings are essential.
In order to confirm the validity of the linear combination method, a test was made with ideally synchronized signals. The artefact signal was synthesized, composing of the three reference signals used for artefact removal. The coefficients were [3.1337, 0.1337, 5.3533]. The coefficients were chosen an order of magnitude different on purpose. The resulting artefact reduction in the order of 10^{-13} times demonstrates the validity of the method for ideally synchronized, noiseless signals
The same synthesized signal can be used as the gradient switching artefact on the microneurography recording. Since the frequency ranges overlap, the microneurography signal is expected to influence the artefact removal process and consequently the method will remove some of the microneurography.

To assess the influence of artefact removal by least squares fit on the final microneurography signal, a test was made where the synthesized artefact signal was added to continuous sine and cosine signals from the same frequency range. One test was also carried out with the real microneurography signal added to the synthesized signal. The coefficients were calculated and corresponding signal subtracted. To see the effect of artefact removal process, the original signals of interest were subtracted from the results. Final noise was obtained and the results in Table 8 show some interference from the artefact removal to the actual signal. The added signals were about one hundred times smaller in amplitude and the artefact removal had an effect of less than 1%. The effect can also be compared by comparing the linear combination coefficients that should be the same as the ones used for calculating the synthesized signal (compare [3.1337, 0.1337, 5.3533] with the values in Table 8). For the real microneurography signal the method worked nearly perfectly.
Since the microneurography signal is much smaller in magnitude than the gradient switching induced in the microelectrode loop, noise from all sources must me minimized. Artefact removal is not expected to remove or reduce the microneurography signal, but insufficient artefact removal leaves some of the gradient switching noise present on the recordings.
The sampling frequency of 50 kHz left the possibility of misalignment of the signals by half a sample or 10 µs. When plotting the linear combination results, the strongest errors remain at the edge of sharp gradient changes. This is probably caused by insufficient time alignment. To reduce the effect of misalignment and high-frequency noise on the recordings, a test was made with different low-pass and high-pass filters applied on the signals. The results demonstrated that while low-pass filtering removes the high frequency noise and improves the result (Table 9), the high-pass filters had no significant result. Removal of the DC component is still important prior to calculating the linear combination.
The filter parameters used in clinical practice should be discussed between clinical doctors and engineers to achieve optimum trade-off between increased artefact attenuation and suppression of the original signals.

5.4 Signal processing with improved time alignment

The importance of synchronization of the signals had been proven and the maximum sampling frequency of the ADC (100 kHz) was used for next measurements. Since the recordings were performed with the orthogonal coils (Figure 16), the signal measured as the artefact signal consisted of three separate signals. For the first artefact removal calculations, they were treated as three different artefact signals. The results in Table 11 show quite strong variation in RMS reduction.
Due to the fact that the results in Table 11 were not significantly better than the results from the first trial of the linear combination method (Table 3, sampling frequency 50 kHz), using time shifted copies of the reference signals was investigated. For each reference signal, two slightly time shifted copies were created by linear upsampling and shifting one of the signals before and the other later by the shifting factor. All together nine reference signals were used for the reconstructions instead of three. The artefact reduction improved remarkably (nearly two times) for one of the signals but remained about the same or provided small improvement for the others.
It must be noted that the same procedure of creating time-shifted copies and using them as additional signals for artefact removal is expected to improve the results for the 50 kHz calculations as well (not tested in the thesis). This means that the sampling

frequency of 50 kHz might be sufficient for the final set-up with simultaneous measurements.
It should be noted that when using nine signals for the artefact removal, the sum of coefficients for one gradient direction (shifted signals and the original), representing the proportion of that certain gradient direction in the artefact signal, remained about the same as before, when using only the original reference signals for artefact removal. The validity of the method and presence of imperfect time alignment between the signals can be concluded.
Figure 38 presents the results after artefact removal for the frequency encoding signal. Figure 37 shows the initial gradient switching signal for one volume. It can be seen that the gradient switching signals recorded in the MR environment have a consistent fluctuation of the peaks (not present on the baseline). The origin of this fluctuation is unknown and attempts to remove it have so far failed. Being consistent in all the recordings it is expected to origin from the MR scanner but due to being out of phase between the measurements, it should not be caused by the pulse sequence. It might be caused by the gradient amplifiers but this has to be confirmed. It might be possible to remove it when synchronizing the signal sampling with the reference clock of the pulse sequence, but that has to be confirmed. Being out of phase between the reference and artefact measurements, it is the main source of final noise after artefact removal as seen in Figure 38. Therefore using simultaneous measurements are essential for recording the fluctuations in phase and making it possible to remove them by the linear combination method.
The validity of the method had been proven for the case when an ideal solution exists. The RMS reduction of the artefact by the factor of 30 had been achieved for signals recorded one after another. The remaining noise has its origin from the gradient switching and follows the activity of the pulse sequence. With simultaneous measurements, remarkably better artefact suppression is expected.
When microneurography data is processed, it is filtered and the moving average of the magnitude is calculated (leaky integration). Since the gradient switching noise will still be present and influence the leaky integrator, the activity areas of the pulse sequence can be misinterpreted as bursts. To further reduce the effect of gradient switching on the final result, an additional electrode loop can be used following the real microneurography electrode loop as closely as possible. This supplementary signal can be processed the same way as the microneurography signal with the gradient switching artefact. It would include the information about the activity areas of the pulse sequence which are not removed by the initial artefact removal.
To see the effect of additional supplementary signal for artefact removal and how much the current set-up has to be improved, a test was made where the artefact signal was synthesized from the three orthogonal signals measured at the knee position. The same synthesized signal was used as an ideal supplementary signal. The three orthogonal references measured on the rear side of the scanner close to the head coil and symmetry axis were used as reference signals along with the slightly time-shifted copies of the same signals.
The microneurography signal was added to the artefact signal and the least squares fit calculated for both the synthesized signal with the microneurography and the supplementary signal. After artefact removal, the signals were filtered and rectified and fed through the leaky integrator as the real microneurography would be processed. Since the supplementary signal was ideal, the best estimation of microneurography was obtained by subtracting the processed result from the artefact removed and processed microneurography result.

It must be noted that the peak-to-peak amplitude ratio between the microneurography signal and the gradient switching artefact was nearly 10^{-4} and SNR nearly 10^{-8}. Using the supplementary signal got the result to be in the same order with the processed microneurography (Figure 41), but the result and result of microneurography differ remarkably. Table 15 presents the results after artefact removal by least squares fit for different amplifications of the microneurography signal.
When the microneurography signal was amplified 10^3 times prior to adding the artefact signal (having the peak-to-peak amplitude ratio of 0,1 and SNR of 0,01), the microneurography can be recognized after artefact removal and subtracting the supplementary signal result (Figure 45). Additionally, when the microneurography signal was amplified 10^4 times prior to adding the artefact signal (having the peak-to-peak amplitude ratio and SNR of about 1), the result after artefact removal is nearly perfect (Figure 46 and 47).

6. Recommendations and ideas for the future developments

First modification to be recommended is using simultaneous measurements. For this new hardware is needed. So far the signals were measured one after another and synchronized manually.

A study should be made where the length of the signals used for artefact removal is varied. Throughout the thesis, the whole seventh volume is used for calculating the coefficients. This means that the signals of about 2,7 – 2,8 seconds recorded with 50 or 100 kHz sampling frequency are used for constructing the overdetermined linear equations system. Using shorter periods of time is expected to improve the artefact suppression because a better least squares fit can be found. On the other hand, shortening the time base poses a threat for removing the microneurography signal as well (due to overlapping frequencies). A tradeoff between artefact removal and signal suppression should be achieved.

Least squares fit is used for calculating the linear combination coefficients throughout the thesis. It minimizes the RMS of the resulting signal after artefact removal and can leave peaks with quite high amplitude on the final result. The amplitude minimization of the artefact removed result is an option still to be tested.

7. Conclusions

The measurements performed in the MR environment proved that the gradient switching signals can be recorded and different parts of the pulse sequence can be recognized. The amplitude of the gradient switching proved to be in the same order with the calculated one.
The importance of perfect time alignment was proven several times with several experiments. Simultaneous measurements are crucial for improving the artefact reduction.
Using more reference signals improved the artefact reduction. The improvement was achieved both with using more reference signals from different measurement positions and using additional, slightly time-shifted copies of the original reference signals for calculating the least squares fit coefficients.
The RMS reduction by the factor of 30 was achieved for signals recorded one after another. For the ideal circumstances, when the artefact was synthesized from the reference signals, the method worked perfectly and the gradient switching artefact was totally removed.
The attempt to reconstruct the microneurography signal for a situation representing real life resulted in poor artefact reduction. A reason for this may have been that the artefact and reference signals were not recorded simultaneously.
The unsuitability of the method has not been proved. Consequently, it can be said that the method of calculating the linear combination coefficients by least squares fit for artefact removal can be further investigated and possibly used in practice.

References

[1] Microneurography: how the technique developed and its role in the investigation of the sympathetic nervous system; Å. B. Vallbo, K.-E. Hagbarth, G. Wallin, 2004

[2] Introduction to Functional Magnetic Resonance Imaging; Principles and Techniques. Second Edition. Richard B. Buxton, 2009

[3] The Basics of MRI. Joseph P. Hornak, Ph.D., eBook available at: http://www.cis.rit.edu/htbooks/mri/inside.htm, last accessed March 2010

[4] The Basics of NMR. Joseph P. Hornak, Ph.D., eBook available at: http://www.cis.rit.edu/htbooks/nmr/inside.htm, last accessed March 2010

[5] Medical Imaging Signals and Systems, Jerry L. Prince, Jonathan M. Links, Pearson Prentice Hall Bioengineering, 2006

[6] Microneurography as a tool in clinical neurophysiology to investigate peripheral neural traffic in humans; T. Mano, S. Iwase, S. Toma; Elsevier 2006

[7] Firing properties of single postganglionic sympathetic neurones recorded in awake human subjects; V. G. Macefield, M. Elam, B. G. Wallin; Elsevier 2001

[8] Matlab 7 Help, The MathWorks, 2007

[9] StatSoft, Inc. (2010). Electronic Statistics Textbook. Tulsa, OK: StatSoft. WEB: http://www.statsoft.com/textbook/, last accessed March 2010

[10] Agilent 54621A/22A/24A/41A/42A Oscilloscopes and Agilent 54621D/22D/41D/42D Mixed-Signal Oscilloscopes, User's Guide, Agilent Technologies, 2002

[11] An Investigation into Occupational Exposure to Electromagnetic Fields for Personnel Working With and Around Medical MRI Equipment, Project VT/2007/017 for the European Commission Employment, Social Affairs and Equal Opportunities DG, 2008

[12] DT9800 Series Data Acquisition Modules Specification Datasheet, Data Translation (Marlboro, Massachusetts, USA)

Appendices

Appendix 1 - Linear combination for artefact removal

	Signal 1	Signal 2	Signal 3	Signal 4
Reference 1	0.0623	0.0626	0.0351	-0.0115
Reference 2	-0.0472	-0.0337	-0.0027	0.0143
Reference 3	-0.0137	-0.0317	0.0196	0.0290
Reference 4	-0.0353	-0.0453	0.0212	0.0498
Maximum value of signal	59.7298	52.0616	55.0731	55.0717
Maximum value of result	13.5523	10.8696	7.1594	6.6957
Amplitude reduction	4.4073	4.7896	7.6925	8.2249
RMS of signal	26.2831	23.2625	6.1966	21.4386
RMS of result	1.3352	1.2899	0.9324	0.6447
RMS reduction	19.6852	18.0338	6.6460	33.2519

Table 3: Coefficients and linear combination evaluation parameters for the noise reduction with four signals recorded on the rear side of the magnet (Reference 1, 2, 3 and 4). The maximum and RMS values are in discrete levels.

	Signal 1	Signal 2	Signal 3	Signal 4
Reference 1	0.0106	-0.0037	0.0662	0.0614
Reference 2	-0.0536	-0.0421	0.0012	0.0235
Reference 3	0.0477	0.0471	-0.0173	-0.0577
Maximum value of signal	59.7298	52.0616	55.0731	55.0717
Maximum value of result	13.2192	12.2749	11.3962	12.2234
Amplitude reduction	4.5184	4.2413	4.8326	4.5054
RMS of signal	26.2831	23.2625	6.1966	21.4386
RMS of result	2.0201	2.335	1.3045	2.2358
RMS reduction	13.0109	9.9596	4.7500	9.5887

Table 4: Coefficients and linear combination evaluation parameters for the noise reduction with three in-plane signals recorded on the rear side of the magnet (Reference 1, 2 and 3). The maximum and RMS values are in discrete levels.

Appendix 2 - Effect of filtering prior to linear combination

	Signal 1	Signal 2	Signal 3	Signal 4
Reference 1	0.0491	0.0328	0.0531	0.0154
Reference 2	-0.0457	-0.0317	-0.0027	0.0134
Reference 4	-0.0289	-0.0297	0.0110	0.0351
Maximum value of signal	60.8359	54.5380	58.0288	58.2749
Maximum value of result	10.3699	9.8932	9.6110	6.7810
Amplitude reduction	5.8666	5.5127	6.0378	8.5938
RMS of signal	26.1804	23.1689	6.1556	21.3515
RMS of result	1.2495	1.3805	0.9930	0.8731
RMS reduction	20.9528	16.7825	6.1992	24.4545

Table 9: Calculation results for Butterworth low-pass filter using passband corner frequency of 6500 Hz, stopband corner frequency of 10 kHz, passband ripple of 3 Db and stopband attenuation of 20 dB. The maximum and RMS values are in discrete levels.

	Signal 1	Signal 2	Signal 3	Signal 4
Reference 1	0.0498	0.0338	0.0527	0.0147
Reference 2	-0.0479	-0.0347	-0.0028	0.0146
Reference 4	-0.0278	-0.0284	0.0111	0.0346
Maximum value of signal	59.0569	52.4462	54.3756	53.8651
Maximum value of result	11.6354	8.4177	9.3952	6.6930
Amplitude reduction	5.0756	6.2305	5.7876	8.0480
RMS of signal	24.0790	21.3181	5.6536	19.6553
RMS of result	1.2955	1.4061	0.9598	0.8724
RMS reduction	18.5863	15.1611	5.8902	22.5312

Table 10: Calculation results for Butterworth high-pass filter using passband corner frequency of 500 Hz, stopband corner frequency of 50 Hz, passband ripple of 3 Db and stopband attenuation of 20 dB. The maximum and RMS values are in discrete levels.

	Signal 1	Signal 2	Signal 3	Signal 4
Reference 1	0.0496	0.0335	0.0531	0.0152
Reference 2	-0.0467	-0.0332	-0.0029	0.0139
Reference 4	-0.0283	-0.0290	0.0111	0.0349
Maximum value of signal	60.0184	52.3892	56.3735	56.7499
Maximum value of result	9.9465	9.5322	9.5737	6.7469
Amplitude reduction	6.0341	5.4960	5.8884	8.4113
RMS of signal	26.2599	23.2408	6.1821	21.4173
RMS of result	1.3213	1.4517	1.0137	0.9004
RMS reduction	19.8736	16.0095	6.0985	23.7872

Table 16: Calculation results for Butterworth low-pass filter using passband corner frequency of 10 kHz, stopband corner frequency of 13 kHz, passband ripple of 3 Db and stopband attenuation of 20 dB. The maximum and RMS values are in discrete levels.

	Signal 1	Signal 2	Signal 3	Signal 4
Reference 1	0.0497	0.0336	0.0531	0.0151
Reference 2	-0.0470	-0.0334	-0.0029	0.0140
Reference 4	-0.0282	-0.0289	0.0111	0.0349
Maximum value of signal	59.9525	52.3718	54.8252	55.2224
Maximum value of result	10.9582	9.4406	9.6262	6.4855
Amplitude reduction	5.4710	5.5475	5.6954	8.5148
RMS of signal	26.2766	23.2564	6.1917	21.4325
RMS of result	1.3455	1.4688	1.0217	0.9151
RMS reduction	19.5290	15.8340	6.0602	23.4219

Table 17: Calculation results for Butterworth low-pass filter using passband corner frequency of 13 kHz, stopband corner frequency of 20 kHz, passband ripple of 3 Db and stopband attenuation of 20 dB. The maximum and RMS values are in discrete levels.

	Signal 1	Signal 2	Signal 3	Signal 4
Reference 1	0.0498	0.0338	0.0527	0.0147
Reference 2	-0.0479	-0.0347	-0.0028	0.0146
Reference 4	-0.0278	-0.0284	0.0111	0.0346
Maximum value of signal	59.0569	52.4462	54.3756	53.8651
Maximum value of result	11.6354	8.4177	9.3952	6.6930
Amplitude reduction	5.0756	6.2305	5.7876	8.0480
RMS of signal	24.0790	21.3181	5.6536	19.6553
RMS of result	1.2955	1.4061	0.9598	0.8724
RMS reduction	18.5863	15.1611	5.8902	22.5312

Table 18: Calculation results for Butterworth high-pass filter using passband corner frequency of 700 Hz, stopband corner frequency of 50 Hz, passband ripple of 3 Db and stopband attenuation of 20 dB. The maximum and RMS values are in discrete levels.

[n,Wn] = buttord(300*2/50000,50*2/50000,3,20);

	Signal 1	Signal 2	Signal 3	Signal 4
Reference 1	0.0497	0.0335	0.0529	0.0150
Reference 2	-0.0471	-0.0335	-0.0028	0.0141
Reference 4	-0.0282	-0.0289	0.0111	0.0348
Maximum value of signal	61.7598	54.6454	57.0477	56.7656
Maximum value of result	11.7393	8.6323	9.2721	6.4718
Amplitude reduction	5.2609	6.3303	6.1526	8.7713
RMS of signal	26.2738	23.2548	6.1718	21.4293
RMS of result	1.3642	1.4831	1.0337	0.9334
RMS reduction	19.2591	15.6801	5.9706	22.9577

Table 19: Calculation results for Butterworth high-pass filter using passband corner frequency of 300 Hz, stopband corner frequency of 50 Hz, passband ripple of 3 Db and stopband attenuation of 20 dB. The maximum and RMS values are in discrete levels.

Appendix 3 - Linear combination with time-shifted copies of the reference signals

Knee site	Horizontal (freq)	Vertical (phase)	z-direction (slice)
Reference vertical	-0.1015	0.0027	-0.2035
+ shiftfactor 0.1	0.0326	-0.1007	0.0665
– shiftfactor 0.1	0.0547	0.1827	0.1308
Reference horizontal	-0.5835	0.1624	-0.0746
+ shiftfactor 0.1	-0.2640	0.0069	-0.0684
– shiftfactor 0.1	0.6685	-0.1073	0.1130
Reference z-direction	0.2075	0.0514	-0.0571
+ shiftfactor 0.1	0.4518	-0.1187	-0.4283
– shiftfactor 0.1	-0.5233	-0.0137	0.3772
Sum of Ref vertical	-0.0142	0.0847	-0.0062
Sum of Ref horizontal	-0.1790	0.0620	-0.0300
Sum of Ref z-direction	0.1360	-0.0810	-0.1082
Maximum value of signal	174.6773	117.6997	69.3010
Maximum value of result	12.7486	5.9940	5.1645
Amplitude reduction	13.7017	19.6363	13.4188
RMS of signal	73.0036	26.8344	12.7845
RMS of result	2.3885	1.3130	0.9950
RMS reduction	30.5652	20.4380	12.8493

Table 12: Linear combination coefficients and noise reduction parameters for the test which used both the original reference signals and the time-shifted copies for artefact removal. The maximum and RMS values are in discrete levels.

Knee site vertical signal	Synchronization 1		Synchronization 2	
Reference vertical	0.0841	0.0027	0.0813	-0.1533
+ shiftfactor 0.1		-0.1007		0.4184
– shiftfactor 0.1		0.1827		-0.1810
Reference horizontal	0.0622	0.1624	0.0618	-0.2582
+ shiftfactor 0.1		0.0069		0.5356
– shiftfactor 0.1		-0.1073		-0.2155
Reference z-direction	-0.0809	0.0514	-0.0801	0.5151
+ shiftfactor 0.1		-0.1187		-0.7563
– shiftfactor 0.1		-0.0137		0.1606
Maximum value of signal	117.6997	117.6997	117.6997	117.6997
Maximum value of result	6.0986	5.9940	26.2285	6.0094
Amplitude reduction	19.2995	19.6363	4.4875	19.5859
RMS of signal	26.8344	26.8344	26.8344	26.8344
RMS of result	1.4115	1.3130	3.4770	1.2638
RMS reduction	19.0108	20.4380	7.7176	21.2337

Table 13: Linear combination coefficients and amplitude and RMS reduction ratios for the vertical signal before and after shifting it by one sample in time. Synchronization 1 is the same one used for previous results in Table 11 and 12.

Appendix 4 - Reconstructions with real microneurography added to the measured signals

	Synthesized signal	Microneurography	Microneurography + artefact
Reference vertical + shiftfactor 0.1 – shiftfactor 0.1 Reference horizontal + shiftfactor 0.1 – shiftfactor 0.1 Reference z-direction + shiftfactor 0.1 – shiftfactor 0.1	-0.0604 -0.0003 0.0736 -0.0991 -0.0651 0.1349 0.0404 -0.0190 -0.0320		-0.0604 -0.0003 0.0736 -0.0991 -0.0651 0.1349 0.0404 -0.0190 -0.0320
Maximum value of signal	133.7199 (mV)	0.0149 (mV)	133.7185 (mV)
Maximum value of result	9.8897 (mV)		9.8963 (mV)
Amplitude reduction by least squares fit	13.5212		13.5120
RMS of signal	56.8208 (mV)	0.0054 (mV)	56.8208 (mV)
RMS of result	2.1632 (mV)		2.1632 (mV)
RMS reduction by least squares fit	26.2673		26.2672
Peak-to-peak amplitude ratio			8.8503e-005
SNR			9.1030e-009

Table 14: Comparison of synthesized signal (used also as supplementary signal), original microneurography signal and the microneurography signal with the added gradient switching artefact (synthesized signal).

Microneurography signal amplification and peak-to-peak value	1 23,60 µV	10 236,0 µV	10^2 2,360 mV	10^3 23,60 mV	10^4 236,0 mV
Reference vertical	-0.0604	-0.0604	-0.0599	-0.0546	-0.0017
+ shiftfactor 0.1	-0.0003	-0.0004	-0.0007	-0.0037	-0.0343
– shiftfactor 0.1	0.0736	0.0736	0.0734	0.0711	0.0482
Reference horizontal	-0.0991	-0.0991	-0.0991	-0.0990	-0.0978
+ shiftfactor 0.1	-0.0651	-0.0651	-0.0651	-0.0653	-0.0675
– shiftfactor 0.1	0.1349	0.1349	0.1349	0.1350	0.1360
Reference z-dir.	0.0404	0.0404	0.0403	0.0396	0.0323
+ shiftfactor 0.1	-0.0190	-0.0190	-0.0190	-0.0185	-0.0138
– shiftfactor 0.1	-0.0320	-0.0320	-0.0319	-0.0317	-0.0290
Maximum value of signal with artefact, (mV)	133.72	133.71	133.58	141.82	255.43
Maximum value of result, (mV)	9.8963	9.9558	10.5507	19.0251	148.3737
Amplitude reduction by least squares fit	13.5120	13.4300	12.6607	7.4545	1.7215
RMS of signal, (mV)	56.8208	56.8208	56.8230	57.0751	78.5065
RMS of result, (mV)	2.1632	2.1639	2.2301	5.8369	54.2556
RMS reduction by least squares fit	26.2672	26.2591	25.4804	9.7784	1.4470
Peak-to-peak amplitude ratio	8.850e-05	8.850e-04	0.0089	0.0885	0.8850
SNR	9.103e-09	9.103e-07	9.103e-05	0.0091	0.9103
Peak-to-peak amplitude ratio after artefact removal	8.921e-04	0.0089	0.0913	0.7462	0.9984
Peak-to-peak amplitude ratio after leaky integrator	4.992e-04	0.0050	0.0498	0.4295	0.9809
SNR after leaky integrator	2.683e-07	2.682e-05	0.0027	0.2011	0.9556

Table 15: Results after artefact removal by least squares fit. Different amplification of the microneurography signal was used prior to adding the artefact signal.
The peak-to-peak amplitude ratio after artefact removal, peak-to-peak amplitude ratio after leaky integrator and SNR after leaky integrator have been calculated by comparing original microneurography result and artefact removed result.